Quarterly Report for
Contract DE-FG36-02ID14418
**Stanford Geothermal Program**
**April-June 2004**

# Table of Contents

# 1. EXPERIMENTAL STUDY OF PHASE TRANSFORMATION EFFECTS ON RELATIVE PERMEABILITIES IN FRACTURES

This project is being conducted by Research Assistant Chih-Ying Chen, Senior Research Engineer Kewen Li and Prof. Roland Horne. The goals of this research are to compare the flow behavior and relative permeabilities difference between two-phase flow with and without phase transformation effects in smooth-walled and rough-walled fractures. During this research, an experimental apparatus was built to capture the unstable nature of the two-phase flow fractures and display the flow structures in real time. Two-phase flow experiments with phase transformation effects (steam-water flow) and without phase transformation effects (nitrogen-water flow) were conducted. The porous medium approach was used to calculate two-phase relative permeabilities. From the results in this study, steam-water relative permeabilities are different from nitrogen-water relative permeabilities. The enhanced steam-phase relative permeability is due to the effects of phase transformation. This shows consistency with some earlier studies in porous media. The nitrogen-water relative permeability is described most appropriately by using the viscous coupling model. However, steam-water flow in the rough-walled fracture, which is coupled with strong phase transformation effects, seems to be represented better by Brooks-Corey relative permeability functions for fractured media ($\lambda \rightarrow \infty$). The results from this study suggest that relative permeabilities accounting for phase transformation effects have to be used in simulations of geothermal and solution gas reservoirs to represent two-phase interactions adequately.

## 1.1 INTRODUCTION

Two-phase flow has long been of interest in earth fluid and energy production, such as in petroleum reservoir and geothermal reservoir engineering. Simulations of these reservoirs need knowledge of relative permeability functions, which have been studied theoretically and experimentally in porous media for two-phase, two-component systems (i.e. oil and water). However, the relative permeability properties of (1) fractured media, and (2) flow with phase transformation effects, are of great importance but are poorly understood. Fractured reservoirs are not only the major reservoirs in geothermal fields, but also represent over 20% of the world's oil reserves (Saidi, 1983). The phase transformation effects are a characteristic of two-phase flows in geothermal reservoirs (steam-water flow) and gas-condensate reservoirs (gas-oil flow). In spite of considerable theoretical and experimental efforts during the last two decades for either one of these two issues, there are still no general models or approaches to describe relative permeability in fractures, either with or without phase transformation effects.

There have been several studies conducted experimentally and theoretically for the steam-water relative permeability. These studies have been done in consolidated or unconsolidated porous media. The results of these studies fell generally into two contradictory populations. Several studies suggested that in porous media, the steam-water relative permeability functions behave similarly to the nitrogen-water (or air-water) relative permeability functions (Sanchez and Schechter 1987; Piquemal 1994). However, another set of studies suggested that steam-water relative permeability functions behave differently from nitrogen-water in porous media (Arihara et al. 1976; Counsil 1979; Verma

1

1986; Satik 1998; Mahiya 1999; O'Connor 2001). Most these studies showed that the steam-phase relative permeability is enhanced in comparison with nitrogen-phase relative permeability. To the best of our knowledge, no steam-water relative permeability results in fractured media have been reported yet due to the difficulties of the steam-water experiments and poor knowledge of fracture modeling for multiphase flows.

In this study, an experimental apparatus was built to capture the unstable nature of the two-phase flow in both smooth-walled and rough-walled fractures. Improved experimental techniques including the measurement of steam and water flow rates, real-time visualization of the flow dynamics and automated image analysis were used. To simplify the problem, this research focused on phase transformation effects on single-component, two-phase flow in a single fracture, by conducting steam-water flow experiments in both smooth-walled and rough-walled fractures. The purposes of this study were to compare the flow behavior and relative permeabilities difference between two-phase flow with and without phase transformation effects and between smooth-walled and rough-walled fractures. These results provide better understanding of the likely reservoir behavior of gas-condensate, solution gas, geothermal and steam injection reservoirs.

## 1.2 BACKGROUND

It has been widely accepted to treat multiphase flow in fractures as a special case of flow in porous media. In porous media, the commonly used equations to model steady-state, laminar, two-phase flow are Darcy's equations. For the water phase, the equation is given as:

$$q_w = \frac{kk_{rw}A(p_i - p_o)_w}{\mu_w L} \tag{1.1}$$

To take the compressibility effect of the gas into account, the gas phase equation must be written in the form (Scheidegger, 1974):

$$q_g = \frac{kk_{rg}A(p_i^2 - p_o^2)}{2\mu_g L p_o} \tag{1.2}$$

where subscripts $w$ and $g$ stand for water and gas, respectively; $p_i$ and $p_o$ are the inlet and outlet pressures; $q$ is the flow rate; $A$ is the cross-section area; $\mu$ is the dynamic viscosity; $L$ is the length; $k$ is the absolute permeability and $k_{rw}$ and $k_{rg}$ are the relative permeabilities of the water and the gas, respectively.

Few published data are available for two-phase flow in fractures. Most of the studies have been done for air-water systems or for water-oil systems. Previous work on multiphase flow in fractures includes Romm's (1966) experiment with kerosene and water through an artificial parallel-plate fracture lined with strips of polyethylene or waxed paper. Romm found a linear relationship between permeability and saturation, $S_w = k_{rw}$, $S_{nw} = k_{rnw}$ such that $k_{rw} + k_{rnw} = 1$ which represents the X-curve behavior (subscript $nw$ stands for the non-

wetting phase). Fourar and Lenormand (1998) assumed that the complexity of the fracture flow can be simplified, in a first approximation, by viscous coupling between the fluids. The fracture is then modeled by two parallel planes with a small aperture. The viscous coupling between fluids is derived by integrating Stokes' equation for each stratum. Identification of the established equations and the generalized Darcy's equations leads to the so-called viscous-coupling model. Pruess and Tsang (1990) conducted numerical simulation of flow through rough-walled fractures. They modeled fractures as two-dimensional porous media with apertures varying with position. Their study showed the sum of the relative permeabilities to be less than 1, the residual saturation of the nonwetting phase to be large and phase interference to be greatly dependent on the presence or absence of spatial correlation of aperture in the direction of flow.

Persoff and Pruess (1995) also performed experiments on nitrogen and water flow through rough-walled fractures (transparent casts of natural fractured rocks). Their study showed that the flow experienced strong phase interference similar to that in porous media. Flow of a phase was characterized by having a localized continuous flow path that undergoes blocking and unblocking by the other phase when the flow rates were small. Diomampo (2001) performed experiments of nitrogen and water flow through both smooth- and rough-walled artificial fractures, and also observed the intermittent phenomenon in her experiments. Diomampo's results conformed mostly to the Corey type of relative permeability curve. This suggests that flow through fractures can be analyzed by treating it as a limiting case of porous medium flow and by using the relative permeability approach.

Regarding steam-water flow in porous media, some of the earliest attempts to measure the steam-water relative permeability were made by Miller (1951), Arihara et al. (1976), Chen (1976) and Council (1979). However, these results have been deemed to be less reliable due to the limitations of measurement techniques at this early stage; for example, their saturation measurements were either absent or inferred from capacitance probes. Later, Verma (1986) improved the saturation measurement by using the gamma-ray densitometer in his steam-water experiment in an artificial sand pack. Verma's results revealed strong enhancement of the steam-phase relative permeability and he remarked that the phase transformation effects lead to more efficient transport of the steam phase and reduce the pressure drop across the flow channels. In the last decade, with the advance of tomographic technology, X-ray CT scanners have been used to determine the saturation distribution for steam-water flow in porous media, by Satik (1998), Mahiya (1999) and O'Connor (2001). Horne et al (2000) summarized Satik's and Mahiya's results and compared them with nitrogen-water flow. Both results agreed qualitatively that the steam-phase relative permeability is higher than that of the nitrogen phase, which is consistent with Verma's results. However, Sanchez and Schechter (1987) and Piquemal (1994) presented contradictory results. Sanchez and Schechter estimated the average water saturation through an entire core of unconsolidated porous medium and ignored the spatial variations in saturation. Their results showed that the steam-water relative permeabilities behaved similarly to those of the nitrogen-water flow. Piquemal (1994) conducted steam-water flow experiments at $180^{\circ}$C in an unconsolidated material packed in a tube 25 cm long and with an internal radius of 5cm. During the experiment, pressure and temperature were measured

at four points along the core holder 5cm apart. The results also suggested that steam-water flows are similar to those of nitrogen and water.

These previous studies show a diversity of behavior of nonboiling relative permeabilities in fractures and steam-water relative permeabilities in porous media. Issues such as whether the phase transformation enhances steam-phase permeability, and how the surface roughness of fractures affects relative permeabilities remain unresolved. The main objective of this study was to contribute to the resolution of these issues. This report is structured as follows: we first describe the detailed design of the apparatus and the automated measurement techniques, as well as the experimental procedures. Next, we report the experimental results, present the flow structure images, and discuss the effects of phase transformation and fracture roughness on relative permeabilities. Finally, we compare our results with earlier studies and summarize the main conclusions of this study.

## 1.3 APPARATUS, MEASUREMENTS AND METHODS

The steam-water flow experiment is more complex than a nitrogen-water experiment because the former has to be performed at high temperature, and there is a fundamental difficulty in measuring how much of the fluid flows as steam and how much as liquid. Furthermore, according to earlier studies, multiphase flows in fractures are inherently unsteady (Persoff and Pruess 1995; Diomampo 2001; Chen et al. 2004). To this end, novel experimental techniques were used to capture the unstable nature of the two-phase flow, to measure the steam and water flow rates directly, to visualize the flow dynamics in real-time and to analyze the images automatically. The whole system was designed to be conducted at an isothermal condition by installing the fracture apparatus inside an air bath, which maintained a constant temperature. All measurements were electronic and digitized by using a high-speed data-acquisition system (National Instrument, SCSI-1000 with PCI 6023E A/D board) and digital video recording system (Sony Digital-8 560X with Pinnacle Studio DV IEEE 1394 image capture card). The whole experiment system is illustrated in Figure 1.1, which shows the deaerated water supply, the fracture apparatus (inside the air bath), data acquisition system, and digital image recording.
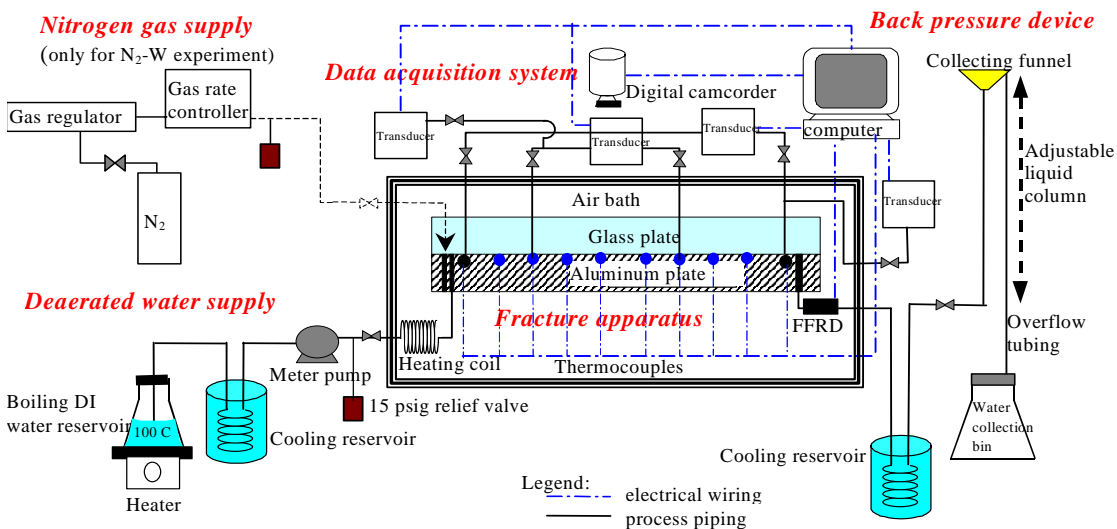


*Figure 1.1: Process flow diagram for steam-water experiment.*

4

### 1.3.1 Fracture Apparatus Description

The fracture was created by mounting a smooth or rough glass plate on top of an aluminum plate, confined by a metal frame bolted to the bottom plate. The frame was designed to hold the seal and to avoid deformation of the glass due to system pressure. Several windows and a mirror attached to the frame allow the flow visualization (see Figure 1.2). The fluids enter the fracture through two separate canals containing a total of 123 capillary ports (diameter 0.02 inch) which align on the surface alternately (see the schematic diagram in Figure 1.2). These capillary ports were used to deliver the fluids to the fracture surface evenly. Throughout the flow area, needle-size temperature ports with the diameter of 0.02 inch were drilled to minimize surface discontinuity. In addition to these ports, four needle-size pressure ports with the same diameter were drilled throughout the flow area. The two-phase fluid exits through a single outlet. The apparatus was designed to be of sufficient length that end effects only affect a small part of the flow window – experimental observations have confirmed this to be true.

For the smooth-walled experiment, a plain glass sheet was used as the top plate. The aperture of the fracture was set by installing the stainless steel shims with thickness 130μm as the fracture spacer. For the rough-walled experiment, a specially designed, rough-walled glass was used as the top plate. The rough glass has a repeating pattern with 160μm maximum vertical variation. An optical surface profilometer (OGP; Optical Gaging Product, SmartScope Avant ZIP video measuring system) was used to determine the profile of the rough surface, which is shown in Figure 1.3. This rough glass was placed above the aluminum bottom plate with thin silicon shims (thickness < 200μm) in between.
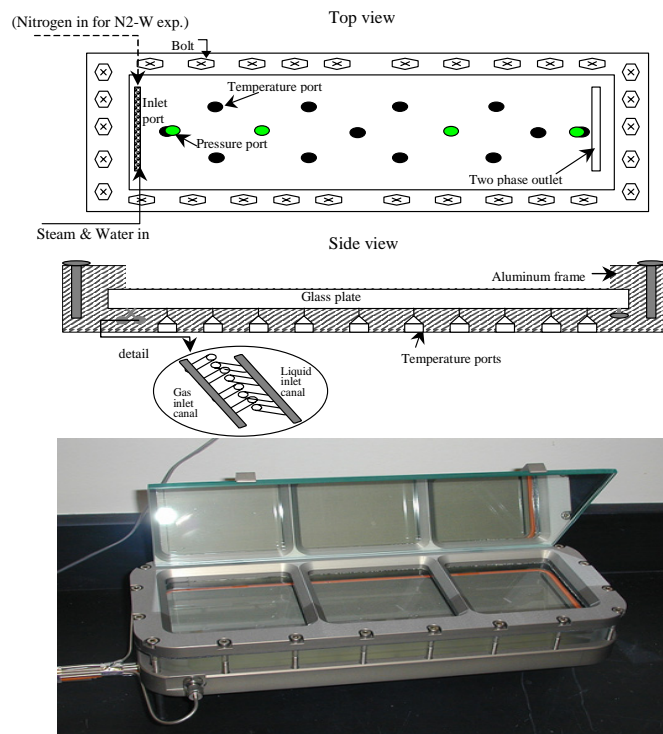


*Figure 1.2: Schematic diagram and picture of fracture apparatus.*
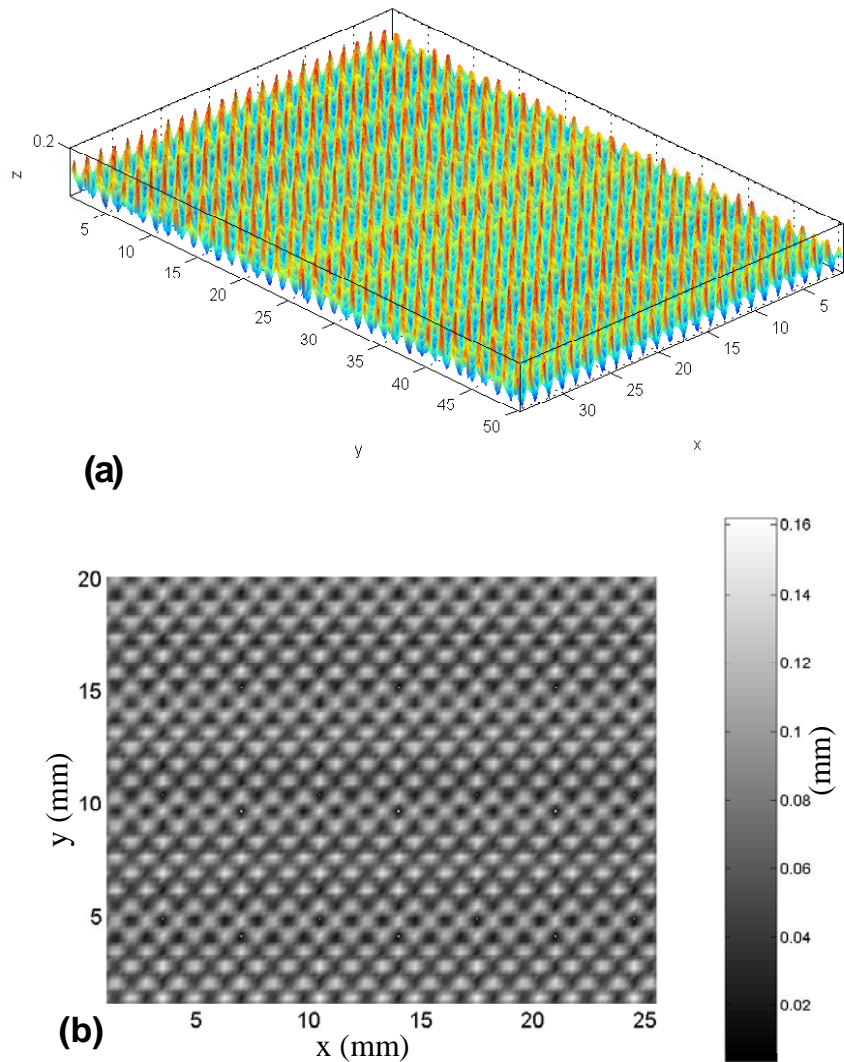
**(a)**



**(b)**

*Figure 1.3: Surface profile of the rough top glass: (a) 3-D profile (height not to scale), (b) 2-D profile.*

### 1.3.2 Flow Rates Measurements

One of the main challenges of the steam-water flow experiment was to measure the steam and water flow rates, since phase transition occurs when steam and water flow through the fracture. Therefore using flow meters to measure the rate of each phase becomes inappropriate, because it is always impossible to separate steam from water without any mass loss or gain. To overcome this situation, an in-situ fractional flow ratio detector (FFRD) was designed and constructed as shown in Figure 1.4a. An LED light source emits visible light beams which pass through the transparent FFRD tubing connected to the outlet of the fracture. A phototransistor (NTE 3038, NPN-Si, Visible, Vcbo 25V, Ic 20mA, Pd 50mW, response time 1.5μs) was installed inside the FFRD, producing different voltages when sensing different strengths of light emitted from the LED. The water phase produces a higher voltage when flowing through the FFRD. In order to minimize the heat loss, the FFRD device was installed as close to the outlet of the fracture as possible (about

6

2 inches distance). To catch the fast and unsteady steam and water segments in the outlet tubing, The FFRD was connected to the high-speed data acquisition system with 250Hz sampling frequency. An example of the FFRD response signal during testing is shown in Figure 1.4b. The calibration of the FFRD is shown in Figure 1.5.
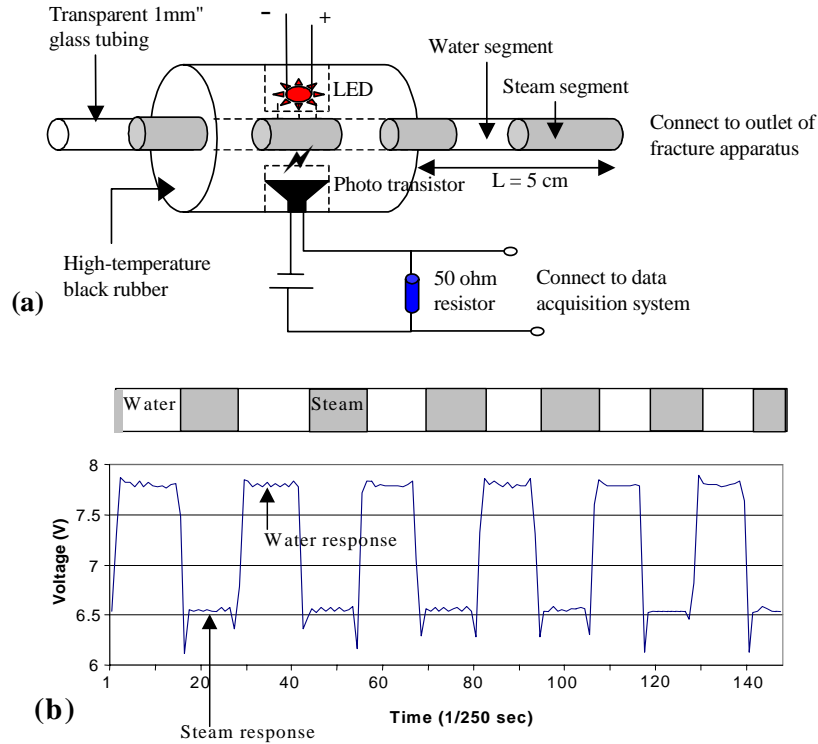


Figure 1.4: Fractional flow ratio detector (FFRD) (a) schematic (after Chen et al. 2004) (b) detected steam and water signal.
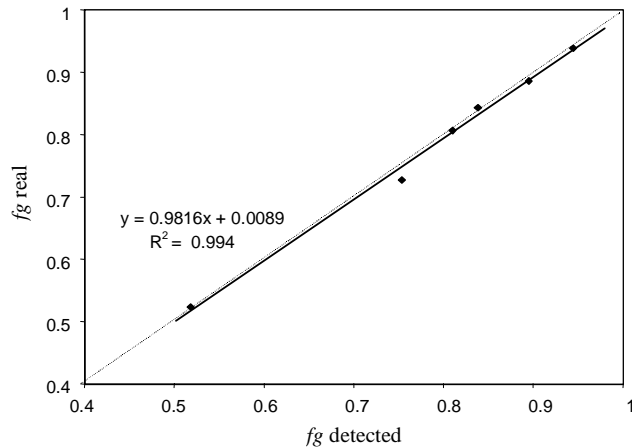


Figure 1.5: FFRD calibration (Fluid: water and nitrogen; FFRD tubing ID: 1.0mm).

Once the steam and water responses are obtained from the FFRD, the statistical histogram is plotted and the steam and water phase flow ratios are obtained by determining the threshold of the histogram. The outlet steam and water fractional flows, $f_s$ and $f_w$, are defined as:

$$f_s = \frac{q_{out,s}}{q_{out,t}} \tag{1.3}$$

$$f_w = \frac{q_{out,w}}{q_{out,t}} \tag{1.4}$$

where $q_{out,s}$ is the output steam flow rate, $q_{out,w}$ is the output water flow rate, and $q_{out,t}$ is the output total flow rate. As $f_s$ and $f_w$ are obtained, it is easy to evaluate $q_{out,s}$ and $q_{out,w}$ by using mass balance if a short-term steady condition is reached. The mass balance equation is:

$$m_{in} = q_{out,t}(f_w \rho_w + f_s \rho_s) \tag{1.5}$$

Substituting Equation (1.5) into Equations (1.3) and (1.4), the end-point steam and water flow rates are then given by:

$$q_{out,w} = f_w \frac{m_{in}}{f_w \rho_w + f_s \rho_s} \tag{1.6}$$

$$q_{out,s} = f_s \frac{m_{in}}{f_w \rho_w + f_s \rho_s} \tag{1.7}$$

The end-point steam quality is:

$$X_o = \frac{\rho_s q_{out,s}}{m_{in}} \tag{1.8}$$

where, $m_{in}$ stands for the input mass, $\rho$ is the density.

The flow rates obtained are end-point flow rates, which may differ from the representative rates due to the pressure and temperature change along the fracture. Therefore, a further calculation is needed to obtain the center-point flow rates. Since the experiments were conducted under near-adiabatic conditions, and the temperature variations across the fracture (30 cm in length) recorded during the steam-water experiments were less than 0.5°C, the heat loss across the fracture was negligible. Using mass and energy balances with flat interface thermodynamics assumption, the steam quality ($X$) in the flow at any position would be given by:

$$X_x = \frac{L_{To}}{L_{Tx}} X_o + \frac{h_{Lo} - h_{Lx}}{L_{Tx}} \tag{1.9}$$

where $L_T$ is the latent heat of vaporization at the prevailing temperature and pressure, and $h_L$ refers to the liquid specific enthalpy, subscripts $o$ and $x$ denote the end-point and section $x$ considered, respectively. The center-point steam quality was used to calculate the center-point flow rates of steam and water.

The limitation of the FFRD method is that if the flow is in an extremely unsteady state, some mixed phase response will occur in the FFRD, and the flow rates calculated will become less accurate. However, if the flow is in quasisteady state (i.e. the steam or water flow rate changes at a fairly slow rate), rates obtained by this method should approximate the real flow rates except for a short delay of the phase response. The experiments were conducted in a sequence of constant pressure steps to minimize the rapid, unstable flow.

### 1.3.3 Saturation Measurements

The instantaneous saturation measurement has long been a major challenge of multiphase flow experiments. The transparent top glass enables us to visualize and videotape the two-phase flow scenes in real time. Still images were then extracted with less than one-second frequency from the digital video recorded during the experiments. These images were synchronized with the logged data through the time read from the LCD monitor. Figure 1.6a shows a typical video image taken from the experiments. The photographs were processed in a computer program that does quadratic discriminant analysis (QDA) to group the pixels of the picture into three groups: the water phase, steam phase and the frame, based on color differences.  Finally, saturation is computed as total pixels of the liquid group over the sum of the steam and liquid groups. Several earlier studies (Pan et al. 1996, Diomampo 2001) used similar techniques for the saturation measurement; however due to the transparent and colorless characteristic of both fluids, they all dyed the liquid phase to enhance the color differences. Dyeing the water may alter the physical and thermodynamic properties, which discouraged us from using this procedure. To obtain distinct color differences between steam and water, a carefully designed lighting system was placed at the rear of the fracture. The light beams pass through the transparent top wall of the fracture (the glass plate) horizontally, which makes the fluids stereoscopic and darkens the gas phase. Figure 1.6b is a gray-scaled image produced by the QDA program from the original cut photograph. Better accuracy has been achieved compared to the results from the dyeing approach.
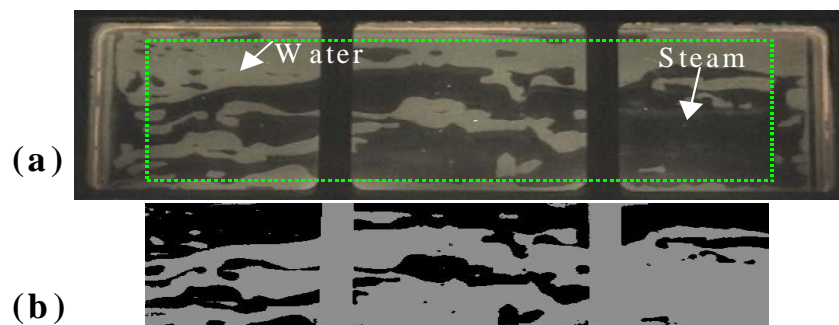


*Figure 1.6: Sample video image taken for steam-water runs and its processed gray scale image used in determining saturation.*

9

### 1.3.4 Pressure Measurement

Capillary end effect was an issue because of the influence on the pressure measurement. In the apparatus, four pressure ports were drilled along the fracture for intermediate pressure difference measurement, to minimize capillary end effect and to facilitate intermediate absolute pressure measurement along the length of the fracture. Another issue that affects the pressure measurement is phase transformation inside the pressure tubing. Since steam-water experiments were conducted at a temperature at the boiling point of water, the water-filled pressure tubing connected to the pressure transducers had a tendency to boil. This means both liquid water and vapor coexist inside the pressure tubing. Insensitive and erratic pressure response was obtained due to the different compressibility in water and gas and the solubility of gas. To resolve this, additional outer cooling tubing was added to cool the pressure tubing to minimize this two-phase phenomenon. This cooling jacket quenches the tubing and maintains the content inside the inner tubing in the liquid phase (water). The plumbing of the pressure measurement is shown in Figure 1.7. Four low-range differential transducers were used to measure the pressure drop through the fracture, as well as the intermediate pressure and the two-phase outlet pressure (Validyne Transducer, model DP-15, range 0-2psi and range 0-5psi). These transducers send electrical signals to the SCXI-1000 data acquisition device, which was monitored using the LabView® virtual instrument program.
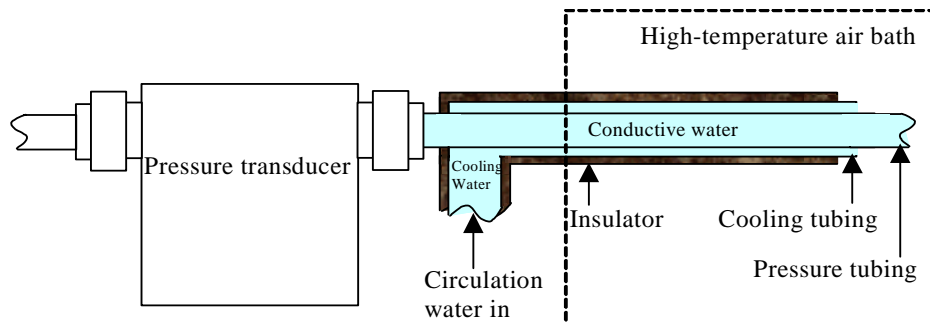


*Figure 1.7: Improved plumbing of the pressure measurement to reduce two-phase problem.*

### 1.3.5 Experimental Procedures

First, single-phase water flow experiments were conducted at room temperature and high temperature to characterize the hydraulic properties of the fractures. After that, the steam-water and nitrogen-water flow experiments were conducted in a drainage process.

For the steam-water experiments, there are two methods available to produce steam-water flow inside the fracture. One method is by injecting steam and water separately into the apparatus. The steam would be produced using a steam generator inside the air bath to boil steam from deaerated water. The other method is by injecting only deaerated water into the apparatus, after which the steam phase is produced by adjusting either pressure or temperature in the fracture to make the water boil. Since the steam quality from a steam generator is hard to control, the heat loss from the steam generator to the fracture apparatus is hard to determine, and there is a significant phase transformation at the moment when the injected steam and water meet in the inlet port, the latter method was used in this

experiment. First, the air bath was heated to $104^{o}$C, and then the fracture was fully saturated with water using a vacuum pump. Next, water was injected using a metered pump (Dynamax, SD-200, rates: 0.1-200 ml/min) which controlled the rate of injection. The water used in the experiment needs to be deaerated almost completely. To reach this quality, distilled water was evacuated using a vacuum pump for 2 hours, and then the water was boiled to achieve a low dissolved-gas condition. The deareated water entered the air bath and then passed through a 6-feet long metal heating coil to reach the air bath temperature and produce two-phase conditions. A physical back-pressure device was connected to the outlet of the apparatus to constrain the pressure inside the fracture as shown in Figure 1.1. At the beginning of the experiment, the fracture pressure was set to be larger than the saturated pressure of water at air bath temperature, and then the fracture pressure was decreased in steps to generate two-phase conditions and increase the magnitude of the steam saturation. Within each pressure step, the two-phase flow data and video were not acquired until a repeatable flow structure and saturation variation were reached. This can reduce the instability of the flow and hence decrease the experimental errors.

For the nitrogen-water experiments, the apparatus and all the measurements were the same as for the steam-water case except for a few modifications. The nitrogen-water experiments were performed at room temperature. Nitrogen gas injection was controlled through a flow regulator (Brooks Instrument, Flow Controller Model 0151E), which was connected to a gas meter (Brooks Instrument, Flow Meter model 5850E, max. rate: 200 ml/min). The nitrogen entered the fracture via a different inlet canal from the water, as shown earlier in Figures 1.1 and 1.2.
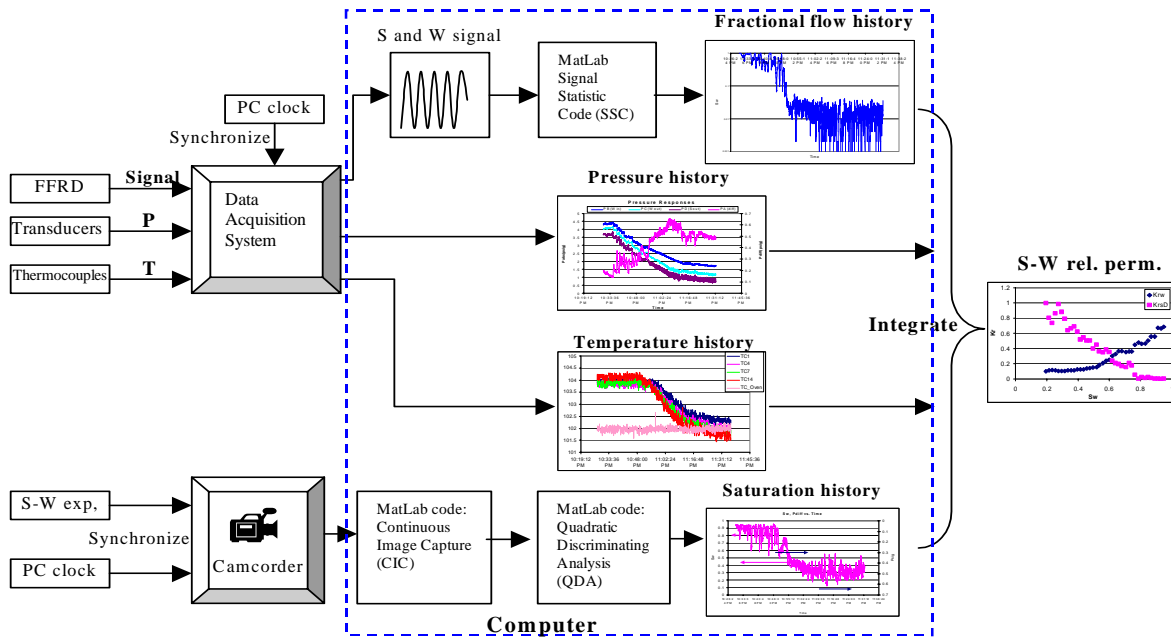


*Figure 1.8: Data and signal processing flowchart.*

11

According to the nitrogen-water experiments reported by earlier studies, the fracture flow experiments are not expected to reach a perfect steady state. Instead, they are unsteady by nature. There are considerable pressure fluctuations accompanied by corresponding saturation changes and the gas and liquid flow rates vary. The design of our system accounted for these issues. The high-speed data acquisition system gathered instantaneous pressure, temperature and flow rate. Instantaneous gathering of saturation data was accomplished by the use of the digital video camcorder and automatic image processing technique with faster than one-second frequency. The methodology and work flow used to integrate all the data and signals and then calculate relative permeabilities is illustrated in the flow chart in Figure 1.8.

## 1.4 RESULTS AND DISCUSSION

### 1.4.1 Hydraulic Properties of the Fractures

Before the two-phase experiment, single-phase flow experiments at $24^oC$ and $90^oC$ were conducted to obtain the absolute permeabilities or the product of absolute permeability and cross-section area, namely the $kA$ parameter. The parameter $kA$ was used in the subsequent calculations for the rough-walled fracture since the cross-section area and the aperture of the rough fracture are not constant. Therefore it is practical to use the combined $kA$ parameter for the relative permeability calculation from Equations (1.1) and (1.2) in the case of the rough-walled fracture. The $90^oC$ values of $k$, $A$ and $kA$ were used to calculate steam-water relative permeabilities (which were actually conducted at $104^oC$), because it is difficult to maintain single-phase flow when the fracture temperature exceeded $90^oC$. Figure 1.9 shows the measured absolute permeability of the smooth-walled fracture at different temperatures and fracture pressures. The absolute permeability of the smooth-walled fracture measured is around 1500 darcies at $24^oC$ and 1400 darcies at $90^oC$ when the fracture pressure is less than 3 psig. The corresponding apertures estimated from cubic law range from 127 to 137μm which are consistent with the fracture spacer installed (130μm). Additionally, the fracture deformation due to the increase of the fracture pressure is small enough to assume constant absolute permeability throughout the smooth-walled experiments.

For the rough-walled fracture, a thin silicon ring was used as the fracture spacer because the stainless steel shims could not seal against leaks due to the surface roughness of the fracture. Though the $kA$ parameter was used to replace the absolute permeability, the corresponding hydraulic aperture could still be estimated by combining the cubic law and Darcy's law:

$$b_h = \sqrt[3]{\frac{12\mu qL}{w\Delta P}}$$

(1.10)

where, $b_n$ is the hydraulic aperture of the fracture, and $w$ is the fracture width. Figure 1.10 shows the $kA$ parameter and estimated hydraulic aperture versus the fracture pressure of the rough-walled fracture at $24^oC$ and $90^oC$. Although our target was to keep the hydraulic aperture of the rough-walled fracture as close as possible to the aperture of the smooth-

12

walled fracture, fracture dilation occurred as its pressure increased due to the flexibility of the silicon ring. However good linearity was observed between the hydraulic aperture and pressure. This fracture dilation is especially obvious in the high-temperature case, because the silicon spacer become more compliant and sensitive to the stress or pressure applied. Therefore, further *kA* parameter correction functions with respect to the fracture pressure were used for the rough-walled relative permeability calculation. The correlation functions are shown in Figure 1.10.
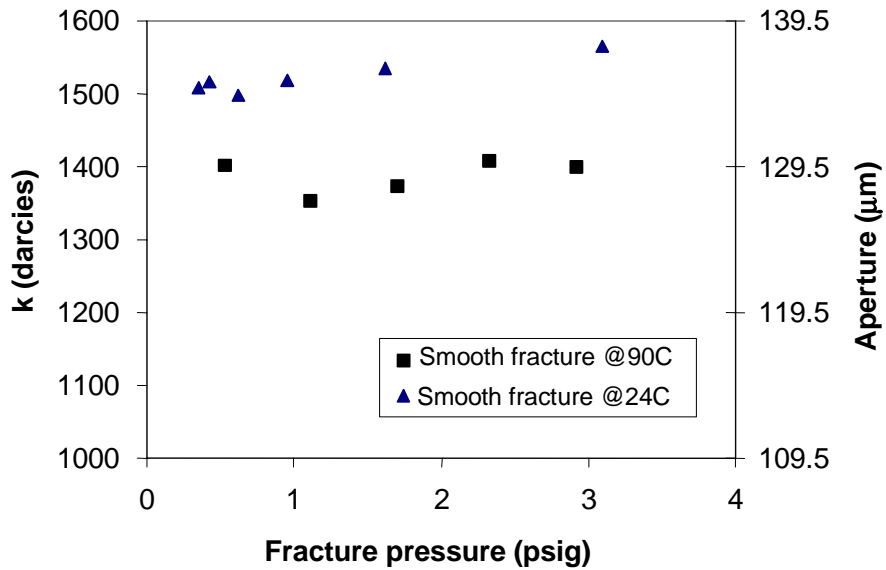


*Figure 1.9: Absolute permeability of the smooth-walled fracture (fracture spacer ~130μm) at different temperature and fracture pressure.*
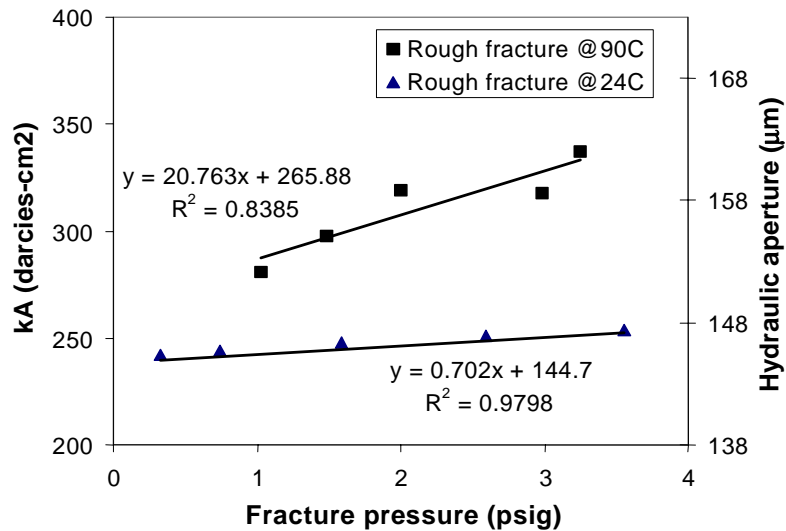


*Figure 1.10: kA parameter and estimated hydraulic aperture of the rough-walled fracture at different temperature and fracture pressure.*

## 1.4.2 Flow Structure and Relative Permeabilities

Figures 1.11 and 1.12 summarize several typical flow structures observed during nitrogen-water and steam-water experiments in both the smooth-walled and rough-walled fractures. Each set of photographs contains a sequence of four snapshots 1 second apart. The photographs in Figure 1.11 have water saturation close to 65%; whereas those in Figure 1.12 have water saturation close to 40%. The flow is from left to right. Gas phase is dark, and liquid phase is light. Generally, nitrogen-water flow forms relative stable aggregate structures in comparison to the steam-water cases in both smooth-walled and rough-walled fractures. The flow structures in the rough-walled fracture always behave in a more scattered, chaotic and tortuous manner in comparison with the smooth-walled case, because the aperture variation tends to trap phases and increase capillary effects. Most of the trapped phases, especially the gas phase, become stationary and contribute to the immobile phase saturation.

In nitrogen-water flow, the nitrogen phase forms fairly stable channels (Figures 1.11a and 1.11c, Figures 1.12a and 1.12c), although those in rough-walled fractures are multibranched and tortuous (Figures 1.11c and 1.12c). On the other hand, almost no stable channels were found in steam-water cases. As can be seen in Figure 1.11b, the steam phase flows as fast moving slugs at $S_w$~65% in the smooth-walled fracture. The shape of the slugs is amorphous. As $S_w$ decreases further, the steam can flow via slugs, bubbles, and channels, whereas the water flows via water slugs, water bubbles, and water channels, as shown in Figure 1.12b. This two-phase cocurrent flow situation was rarely seen in the nitrogen-water case. Considering the effect of fracture roughness, the mobile and immobile steam and water phases distributed more evenly through the flow area in the rough-walled fracture (Figures 1.11d and 1.12d) than in the smooth-walled fracture (Figures 1.11b and 1.12b). This can be attributed to the capillary trapping mechanism and the on-site steam bubble nucleation throughout the fracture space. The latter mechanism occurs much more evenly in the rough-walled fracture.

As mentioned previously, the automated high-speed data acquisition system and digital video processing enabled us to acquire the pressure, temperature, flow rates and saturation data with less than one-second frequency. The comprehensive, high-resolution relative permeabilities were calculated based on these acquired data using Equations (1.1) and (1.2). Figure 1.13 shows the comprehensive collection of steam-water and nitrogen-water relative permeabilities in the smooth-walled and rough-walled fractures. One set of the data was presented previously by Chen at al. (2004). All of these results are scattered. This scattered effect is associated with the fluctuating and unstable nature of the multiphase flow. The detailed interpretation of these results will be presented next with respect to phase transformation effects (steam vs. nitrogen) and surface roughness (smooth-walled fracture vs. rough-walled fracture).
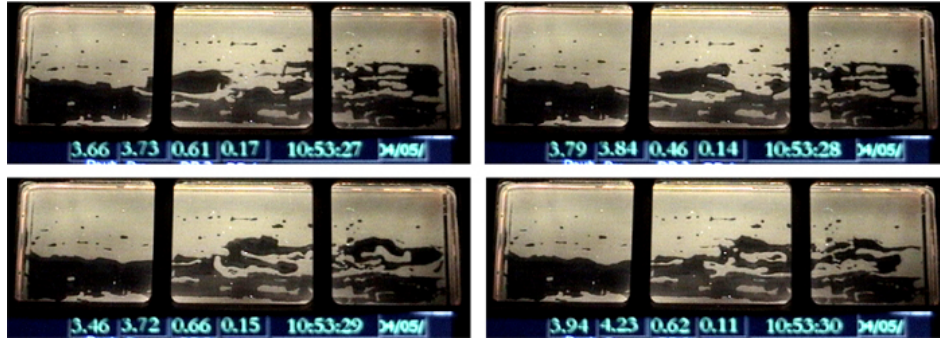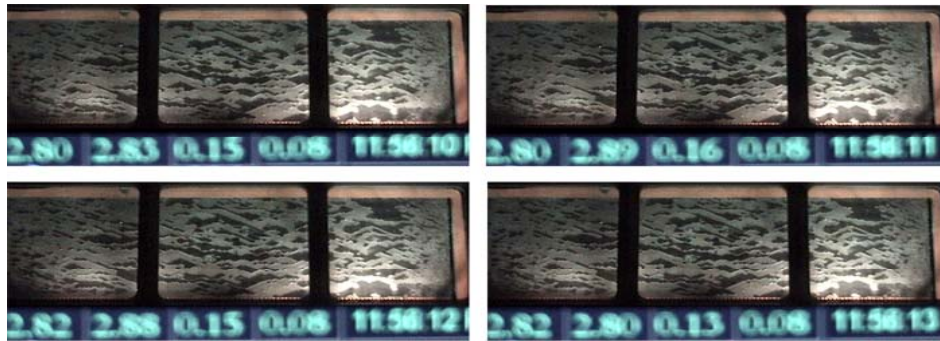
*(a) Smooth-walled, nitrogen-water flow (Sw~65%)*
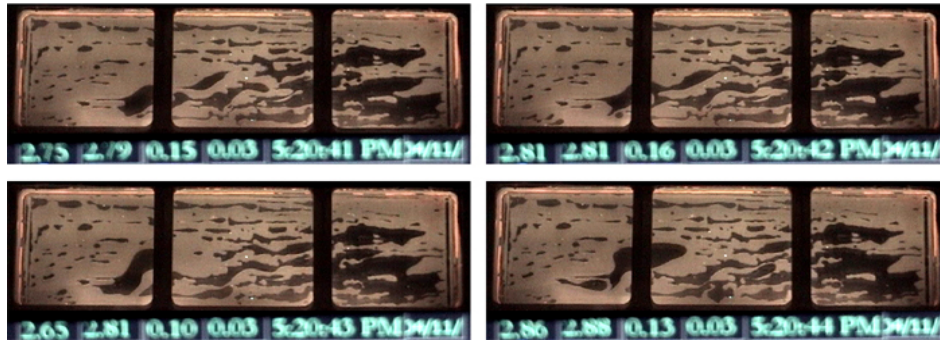


*(b) Smooth-walled, steam-water flow (Sw~65%)*
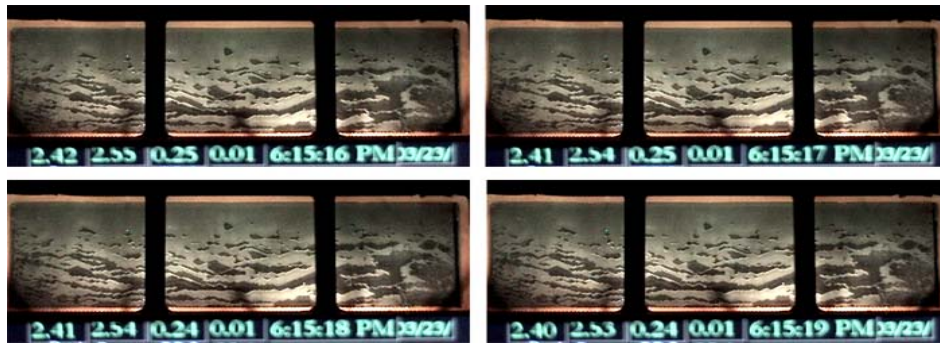


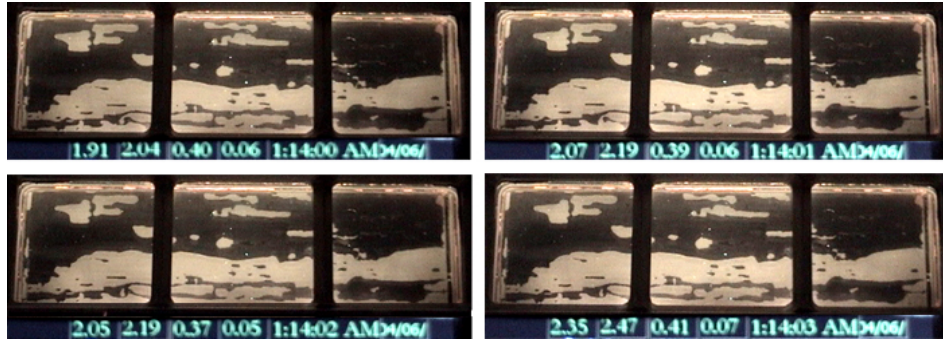*(c) Rough-walled, nitrogen-water flow (Sw~65%)*



*(d) Rough-walled, steam-water flow (Sw~65%)*

*Figure 1.11: Sequence of snap-shots of nitrogen-water and steam-water flow behavior in smooth-walled and rough-walled fractures under 65% water saturation. The flow is from left to right. Gas phase is dark, liquid phase is light. Frame interval is one second.*

*(a) Smooth-walled, nitrogen-water flow (Sw~40%)*



*(b) Smooth-walled, steam-water flow (Sw~40%)*



*(c) Rough-walled, nitrogen-water flow (Sw~40%)*



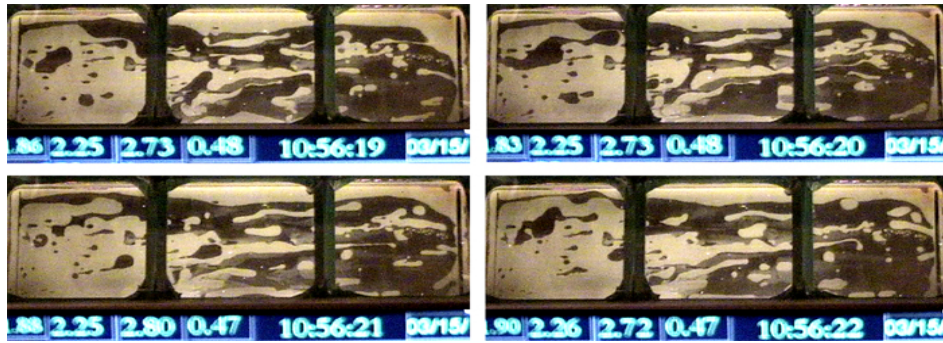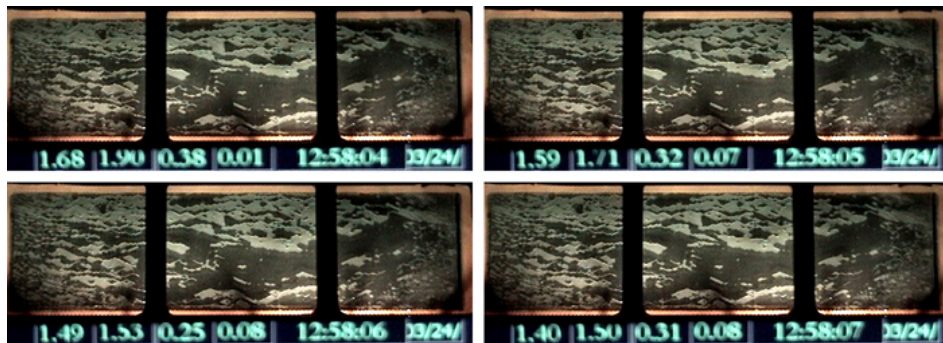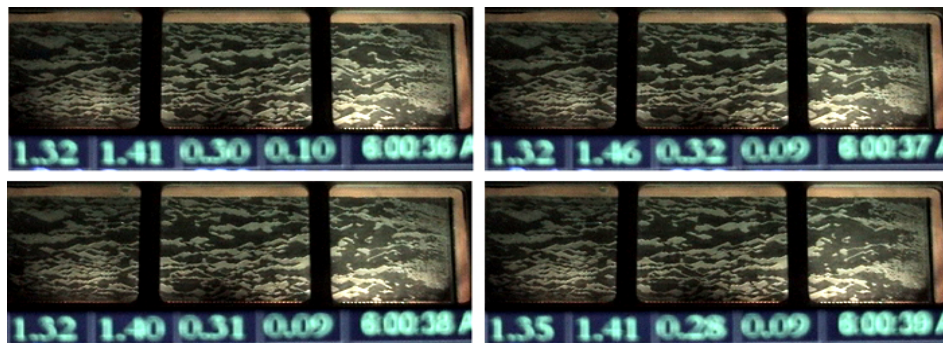*(d) Rough-walled, steam-water flow (Sw~40%)*

*Figure 1.12: Sequence of snap-shots of nitrogen-water and steam-water flow behavior in smooth-walled and rough-walled fractures under 40% water saturation. Frame interval is one second.*
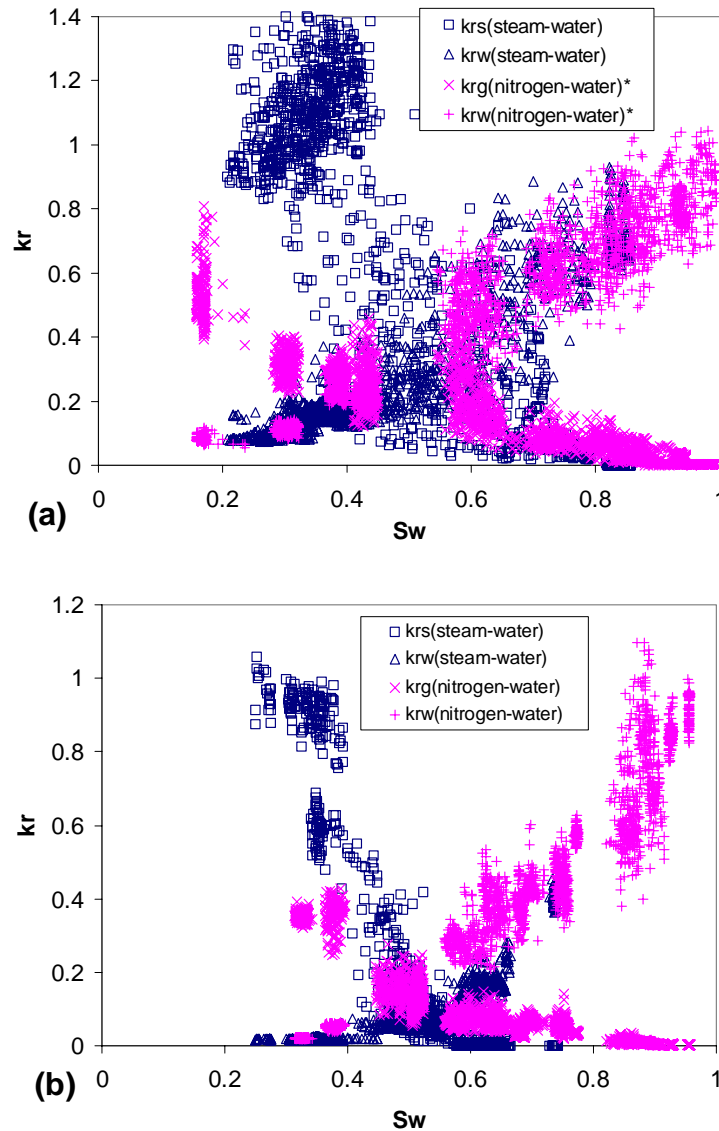
*Figure 1.13: Comprehensive steam-water and nitrogen-water relative permeabilities: (a) smooth-walled fracture, (b) rough-walled fracture. ( \* after Chen et al. 2004)*

### 1.4.3 Effects of Phase Transformation

To gain better visual recognition, averaging techniques were applied to the comprehensive results in Figure 1.13. Figure 1.14 compares the average relative permeabilities between steam-water and nitrogen-water cases in smooth-walled and rough-walled fractures. Two repeated experiments were conducted for the steam-water flow in the rough-walled fracture to demonstrate the repeatability as shown in Figure 1.14b. The curves on both plots show the approximate trends of the data. In the smooth-walled fracture (Figure 1.14a), the liquid curves have similar trends, but the gas curves behave very differently. The steam curve shows a much more mobile character than the nitrogen curve when $S_w <$ *0.6*, which can be seen from the higher relative permeability values in the steam curve. The small portion of initial immobile steam saturation, $S_{si}$, was due to the trapped steam phase

17

stemming from on-site nucleation. Despite the fact that all of these experiments ware conducted in the drainage process, and steam was generated from the heating coil and then injected to the fractures accompanied by water, an initial immobile steam saturation $S_{si}$ was still seen. This nucleation of the vapor phase through the fracture occurs when the liquid approaches its saturation condition. This is one of the distinct characteristics of steam-water flow.
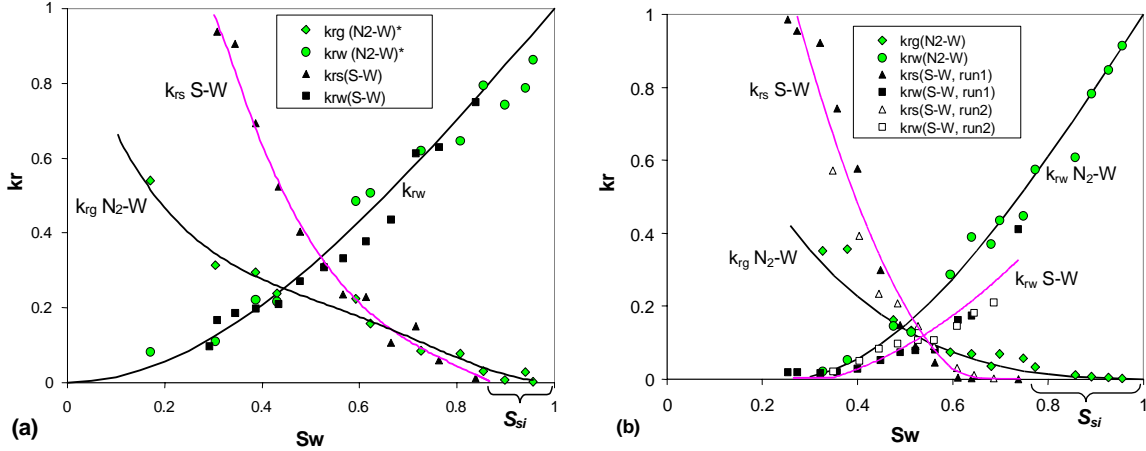


*Figure 1.14: Comparison of average steam-water and air-water relative permeabilities: (a) smooth-walled fracture, (b) rough-walled fracture. ( * after Chen et al. 2004)*

For the rough-walled results (Figure 1.14b), the amount of initial immobile steam increases ($S_{si} \sim 0.25$), because the rough surface enhances the capillary trapping mechanism and on-site nucleation of steam bubbles. According to thermodynamics and surface chemistry studies, the cavities and protrusions on the rough surface are favored locations for the formation of bubbles. Since the rough glass used in this study is homogeneously textured, the trapping and nucleation mechanism occurs evenly, as can be seen from the photographs in Figures 1.11d and 1.12d. These trapped steam islands, characterized by small size and random shapes, scatter over the fracture space and therefore increase the resistance of the water flow and lower the water-phase curve for the steam-water case as shown in Figure 1.14b. Once more, the steam curve shows a more mobile characteristic than the nitrogen curve when $S_w < 0.5$, which shows consistency with the smooth-walled case. The phenomenon of enhanced steam mobility was also observed from the digital images. Under similar water flow rates and saturations, steam slugs tend to move faster than nitrogen slugs, which is the effect of the phase transformation. Some earlier studies proposed that the phase transformation effects lead the vapor phase to advance more efficiently and reduce the pressure drop across the flow channels, thus increasing steam permeability (Verma, 1986). These effects were also observed and attributed to the condensation-vaporization effects with flux "short-circuiting" at liquid islands in unsaturated soils (Walker et al. 1981). However, no clear theoretical or numerical results have confirmed these effects, to the best of our knowledge. Despite this, the enhancement of steam-phase relative permeability shows consistency with some of the experimental measurements in porous media, including those done by Arihara et al. (1976), Verma (1986), Satik (1998), Mahiya (1999) and O'Connor (2001).

## 1.4.4 Effects of Surface Roughness

To evaluate the effect of the surface roughness, Figure 1.14 was replotted for the same fluids but with different fracture roughness. As can be seen in Figure 1.15a, the water curve for nitrogen-water flow is lower for the rough-walled fracture and its residual water saturation increases due to the capillary trapping mechanism mentioned before and also seen in Figure 1.12c. On the other hand, the lowering of the gas curve is not as clear. Figure 1.15b compares the steam-water relative permeabilities between the rough-walled fracture and smooth-walled fracture. The effects of the roughness are similar to the nitrogen-water case, but the magnitude of the differences seems to increase. From Figure 1.15b, the rougher the fracture is, the more the phase interference and smaller the relative permeabilities. Moreover, the initial immobile steam saturation increases in the rough-walled case due to more extensive on-site nucleation and subsequent trapping on the rough surface.
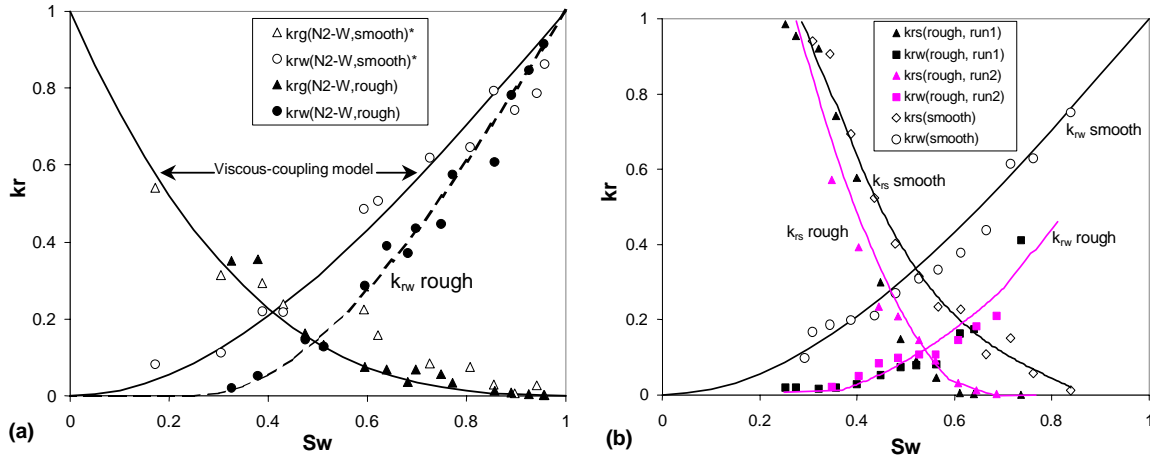


*Figure 1.15: Comparison of average relative permeabilities in the rough-walled fracture with those in the smooth-walled fracture: (a) nitrogen-water flow, (b) steam-water flow. ( * after Chen et al. 2004)*

## 1.4.5 Relative Permeability Interpretations

Several empirical and theoretical models have been proposed to represent the relative permeability in porous and fractured media. In porous media, the Brooks-Corey model has been widely used for modeling two-phase relative permeability and capillary pressure. The Brooks-Corey relative permeability functions are given as:

$$k_{rw} = (S_w^*)^{(2+3\lambda)/\lambda} \tag{1.11}$$

$$k_{rg} = (1 - S_w^*)^2 [1 - (S_w^*)^{(2+\lambda)/\lambda}] \tag{1.12}$$

In these equations, $S_w^*$ is the normalized water saturation defined by:

19

$$S_w^* = \frac{S_w - S_{wr}}{1 - S_{wr} - S_{gr}} \tag{1.13}$$

where subscript $r$ refers to residual saturation, and $\lambda$ is the pore size distribution index. Brooks and Corey (1966) reasoned that media with a wide range of the pore size distribution should have small values of $\lambda$. On the other hand, media with a uniform pore size could have $\lambda$ values close to infinity (Brooks and Corey 1966; Corey 1986). The value of $\lambda$ equals 2 for typical porous media, which reduces the Brooks-Corey model to the Corey model. In the rough-walled fracture, the behavior of the two-phase flow might be approximated to that in porous media. According to Brooks and Corey's reasoning, the value of $\lambda$ should approach infinity in the case of fractured media. Therefore, Equations (1.11) and (1.12) were modified as $\lambda \to \infty$ which leads to the extreme behavior of the Brooks and Corey model for fractures:

$$k_{rw} = (S_w^*)^3 \tag{1.14}$$

$$k_{rg} = (1 - S_w^*)^3 \tag{1.15}$$

In studies of fracture flow and pipe flow models, the earliest fracture model proposed was the linear model (X-curve) which assumed no phase interference between the two phases (Romm 1966). However, many studies confirmed that this ideal situation seemed impossible to achieve in real fractures (Fourar et al. 1993; Chen et al. 2004). Subsequently, some fracture models were suggested based on representing the flows in fractures as flows in two ideal parallel planes. Fourar and Lenormand (1998) assumed that the complexity of the real flow in the fracture can be modeled, to a first approximation, by viscous coupling between the fluids, which is derived by integrating Stokes' equation for each stratum. Identification of the established equations and Equations (1.1) and (1.2) leads to the so-called viscous-coupling model:

$$k_{rw} = \frac{S_w^2}{2}(3 - S_w) \tag{1.16}$$

$$k_{rg} = (1 - S_w)^3 + \frac{3}{2}\mu_r S_w (1 - S_w)(2 - S_w) \tag{1.17}$$

where $\mu_r = \mu_g / \mu_w$ is the viscosity ratio.

As shown in Figure 1.15a, the viscous-coupling model describes the results fairly well for the nitrogen-water relative permeabilities in this study except for the water curve in the rough-walled case. The residual and trapped water in the rough-walled case may violate the assumption of the viscous-coupling model in which no residual phases were

considered. To resolve this, a modified water-phase relative permeability function based on the normalized water saturation $S_w^*$ from Equation (1.13) were used:

$$k_{rw} = \frac{(S_w^*)^2}{2}(3 - S_w^*)$$

(1.18)

This function, shown as the dashed line in Figure 1.15a, agrees with the water curve in the rough-walled fracture. However, the viscous-coupling model cannot describe the steam-water results satisfactorily.

Currently, no theoretical models have been reported to describe the steam-water relative permeability, owing to the complexity of modeling the phase transformation effects and including the thermodynamic and surface chemical properties of both steam and water. Therefore, a unique model for steam-water relative permeability in fractures was not attempted in this research; however, a qualitative comparison of the steam-water relative permeability with the existing traditional models can aid to explore the behavior of steam-water relative permeabilities further. As shown in Figure 1.16, the Brooks-Corey model from Equations (1.14) and (1.15) can describe the experimental steam-water relative permeability in the rough-walled fracture agreeably by setting reasonable residual saturations ($S_{wr}=0.25$, $S_{gr}=0.15$), whereas other models, the linear and viscous-coupling models, cannot. However, the Brooks-Corey model could not describe the water-phase relative permeabilities in the smooth-walled fracture satisfactorily, as shown in Figure 1.17. Li and Horne (2002) suggested that for the steam-water flow in porous media, the steam-phase relative permeabilities could be represented by the Brooks-Corey model, whereas the water-phase relative permeabilities were represented better by the Purcell model which is given as:

$$k_{rw} = (S_w^*)^{(2+\lambda)/\lambda}$$

(1.19)

As $\lambda \to \infty$ for the fracture case, Equation (1.19) is reduced to the normalized linear curve:

$$k_{rw} = S_w^*$$

(1.20)

Figure 1.18 shows a comparison of the steam-water relative permeabilities in the smooth-walled fracture to the Brooks-Corey model (Equation 1.15) for the steam phase and the Purcell model (Equation 1.20) for the water phase. As can be seen, this combined model describes the smooth-walled results satisfactorily.
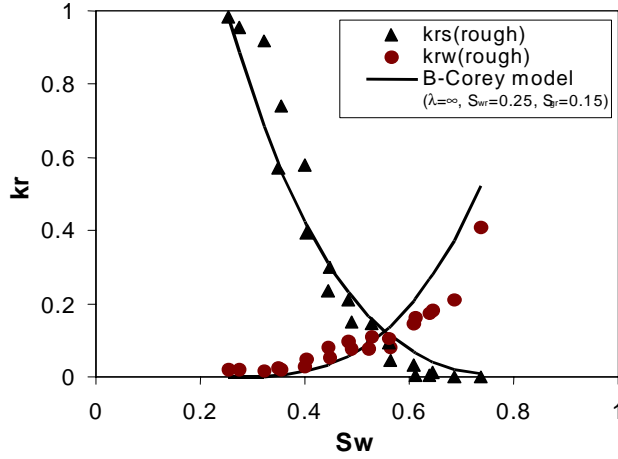
*Figure 1.16: Comparison of average steam-water relative permeability in the rough-walled fracture to the Brooks-Corey model ($\lambda = \infty$, $S_{wr}=0.25$, $S_{gr}=0.15$).*



*Figure 1.17: Comparison of average steam-water relative permeability in the smooth-walled fracture to the Brooks-Corey model ($\lambda = \infty$, $S_{wr}=0.29$, $S_{gr}=0$).*

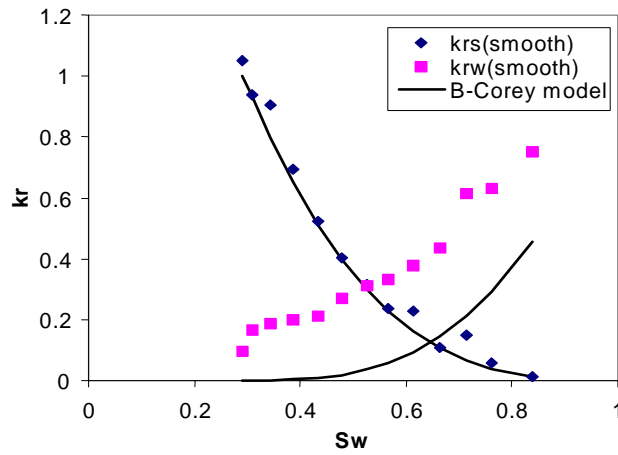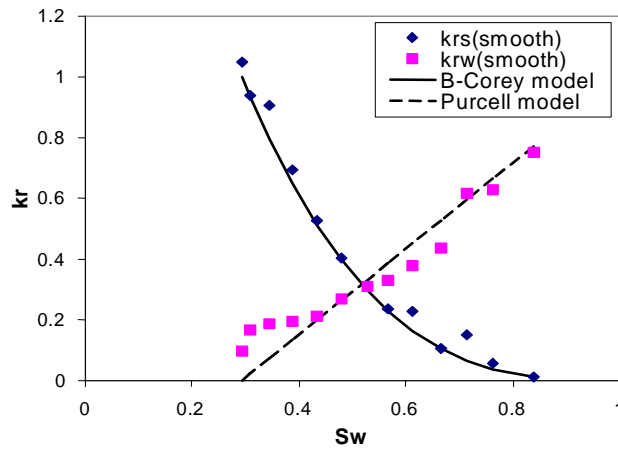

*Figure 1.18: Comparison of average steam-water relative permeability in the smooth-walled fracture to the Brooks-Corey model for the steam phase and Purcell model for the water phase ($\lambda = \infty$, $S_{wr}=0.29$, $S_{gr}=0$).*

Since there are no experimental studies of steam-water flow in fractures reported, to the best of our knowledge, a preliminary comparison of the steam-water results in the rough-walled fracture with earlier studies in porous media was made. As shown in Figure 1.19, the result from the rough-walled fracture conforms to most of the porous media results. The water-phase relative permeabilities have the same trend for all four studies. The steam-phase relative permeabilities from the rough-walled fracture behave similarly to Satik's and Mahiya's results (Satik, 1997 and Mahiya 1999) both of which also showed that the steam-water relative permeability in porous could be interpreted using the Brooks-Corey model. On the other hand, the steam-phase result from Sanchez and Schechter (1987) shows less enhancement and a lower trend. Sanchez and Schechter asserted that there is no distinct difference between the steam-water and nitrogen-water relative permeabilities in unconsolidated porous media and suggested that the steam permeability may be represented accurately by nitrogen permeability under conditions of two-phase flow. This contradicts our results from the rough-walled fracture.
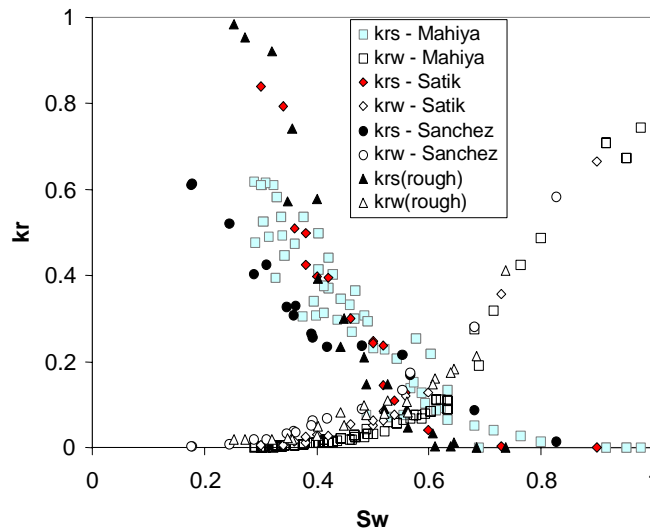


*Figure 1.19: Comparison of average steam-water relative permeability in the rough-walled fracture with earlier studies of steam-water relative permeability in porous media*

## 1.5 CONCLUSION

An experimental apparatus equipped with real-time visualization of the flow dynamics has been built to model steam-water flow in both smooth-walled and rough-walled fractures. Improved experimental techniques for instantaneous steam and water flow rate measurement, high-speed data acquisition and automated image analysis were developed to capture the unstable behavior of gas-liquid flow in fractures.

The steam-water flow behavior in fractures is different from that of nitrogen-water flow. In the smooth-walled fracture, steam and water can flow in multiple patterns (bubbles, slugs and channels) simultaneously and both phases can flow concurrently; however, they never form stable flow structures. Contrarily, nitrogen and water have the tendency to form their

own flow paths and block each other. Due to the capillary trapping mechanism, more immobile phase was found in the rough-walled case, as expected. The flow structures in the rough-walled fracture are much more complex than in the smooth-walled fracture, which may replicate the flow in real rock fractures or joints. Extensive steam nucleation on the rough-walled surface was observed from the flow video. This effect generates the initial immobile steam saturation, which is one distinct characteristic of the steam-water flow. Some of these nucleated steam bubbles are trapped as immobile phase on the rough surface. This contributes to the steam phase saturation and interferes with the water-phase flow.

According to the results from both fractures, steam-water relative permeabilities are different from nitrogen-water relative permeabilities. Steam-phase curves show less phase interference in comparison to the nitrogen-phase curves, which can be attributed to the effects of phase transformation. This enhanced steam permeability shows consistency with most earlier studies in porous media. Comparing with previous steam-water studies in porous media, the steam-phase relative permeabilities in the rough-walled fracture behave similarly to both Satik's and Mahiya's results. By modifying the Brooks-Corey relative permeability functions to expressions for fractured media ($\lambda \rightarrow \infty$), the steam-water relative permeability in the rough-walled fracture seems to be represented satisfactorily by such expressions, and the smooth-walled result can be represented by combined Brooks-Corey and Purcell model as suggested earlier. This may indicate that the multiphase flow with the phase transformation effects can be modeled via the porous medium approaches.

The nitrogen-water relative permeabilities in both smooth-walled and rough-walled fractures are well-described by the viscous-coupling model after this model is modified to account for the residual water saturation; however this model failed to represent the steam-water results in the rough-walled fracture. This implies that the ideal assumption of parallel-plates with simple viscous coupling between fluids can no longer describe the complex flow structures formed by both rough-walled fractures and steam-water flow.

## 1.6 NOMENCLATURE

$A =$ cross-section area of fractures, $L^2$
$b =$ fracture aperture, L
$b_h =$ hydraulic aperture of rough fractures, L
$f =$ fractional flow
$h_L =$ liquid specific enthalpy, Energy/m
$k =$ absolute permeability, $L^2$
$k_{rg} =$ relative permeability of gas phase
$k_{rs} =$ relative permeability of steam phase
$k_{rw} =$ relative permeability of water phase
$L =$ fracture length, L
$L_T =$ latent heat of vaporization, Energy/m
$m_{in} =$ input mass, m
$p =$ pressure, $m/Lt^2$

$q$ =   volumetric flow rate, $L^3/t$
$S_g$ =   gas saturation
$S_{gr}$ =   residual gas saturation
$S_s$ =   steam saturation
$S_{si}$ =   initial immobile steam saturation
$S_w$ =   water saturation
$S_{wr}$ =   residual water saturation
$S_w^*$ =   normalized water saturation
$w$ =   fracture width, L
$X$ =   steam quality

*Greek Letters*

$\mu$ =   fluid viscosity, m/Lt
$\lambda$ =   pore size distribution index
$\rho$ =   density, $m/L^3$

*Subscripts*

$g$ =   gas phase
$i$ =   input
$nw$ =   nonwetting phase
$o$ =   output
$r$ =   residual
$s$ =   steam phase
$t$ =   total
$w$ =   water or wetting phase

## 2. VERIFICATION AND APPLICATION OF A UNIVERSAL CAPILLARY PRESSURE MODEL

This research project is being conducted by Senior Research Engineer Kewen Li and Prof. Roland Horne. The objective of this project is to develop and test a capillary pressure model for use in geothermal reservoir engineering calculations.

### 2.1 SUMMARY

A universal capillary pressure model was developed from fractal modeling of a porous medium and verified using the experimental data from rock samples from The Geysers geothermal field. The capillary pressure data were measured using a mercury intrusion technique. The results showed that the universal model could represent the capillary pressure curves of The Geysers rock satisfactorily while the frequently-used Brooks-Corey capillary pressure model could not. The values of fractal dimension, a representation of rock heterogeneity, were inferred from the match of the universal capillary pressure model to the experimental data.

### 2.2 INTRODUCTION

Capillary pressure plays an important role in geothermal reservoirs. As an example, Tsypkin and Calore (1999) developed a mathematical model of steam-water phase transitions with capillary forces included. They investigated the main characteristics of the vaporization process and found that capillary pressure can play a stabilizing role for the vaporization front, causing a sharp front to develop. Urmeneta et al. (1998) also studied the role of capillary forces in the natural state of fractured geothermal reservoirs and found that capillary pressure tended to keep the vapor phase in the fractures and the liquid phase in the matrix. The numerical results from Urmeneta et al. (1998) showed that capillary forces control the transfer of fluids between fractures and matrix, the stability of the liquid-dominated two-phase zone, and the distribution of steam and water in geothermal reservoirs. This shows that the magnitude of capillary pressure will influence the estimation of the energy reserves and the production performance.

It is essential to represent capillary pressure curves properly because of the important role that capillary pressure plays in geothermal reservoirs. However Li and Horne (2003) found that the frequently-used Brooks-Corey model (1964) could not represent the capillary pressure curves of The Geysers rock samples satisfactorily. The main reason may be that The Geysers rock has many microfractures. Later, Li (2004) developed a universal capillary pressure model theoretically from fractal modeling of a porous medium. The main purpose of the current study was to verify the universal capillary pressure model using experimental data from rocks taken from The Geysers geothermal field.

### 2.3 METHODOLOGY

A brief description of the universal capillary pressure model developed by Li (2004) is discussed in this section. The model is expressed as follows:

$$P_c = [p_{max}^{-\lambda} - (p_{max}^{-\lambda} - p_e^{-\lambda})S_w^*]^{-\frac{1}{\lambda}} \qquad (2.1)$$

where $p_{max}$ is the maximum capillary pressure at $S_{Hg,max}$, which is the maximum mercury saturation; $p_e$ is the entry capillary pressure; $\lambda$ is the pore size distribution index ($\lambda = 2 - D_f$); $D_f$ is the fractal dimension; $s_w^*$ is the normalized wetting-phase saturation, defined as follows:

$$S_w^* = \frac{S_w - S_{wr}}{1 - S_{wr}} \qquad (2.2)$$

where $S_w$ is the wetting-phase saturation and $S_{wr}$ is the residual saturation of the wetting-phase. Air is the wetting-phase and mercury is the nonwetting-phase in the case of measuring capillary pressure using a mercury intrusion technique.

Eq. 2.1 can be reduced as follows:

$$P_c = p_{max}(1 - bS_w^*)^{-\frac{1}{\lambda}} \qquad (2.3)$$

where $b$ is a constant and is expressed as follows:

$$b = 1 - (\frac{p_e}{p_{max}})^{-\lambda} \qquad (2.4)$$

For $D_f<2$, if $p_{max}$ approaches infinity, then Eq. 2.1 can be reduced to:

$$P_c = p_e(S_w^*)^{-\frac{1}{\lambda}} \qquad (2.5)$$

Eq. 2.5 is the frequently-used Brooks-Corey model, which was proposed empirically by Brooks and Corey (1964).

According to this derivation, one can see that the Brooks-Corey capillary pressure model has a solid theoretical basis. This may be why the Brooks-Corey model has been seen to be a good fit to capillary pressure curves of many rock samples.

In the case in which $b=1$, Eq. 2.1 can be reduced to:

$$P_c = p_{max}(1 - S_w^*)^{-\frac{1}{\lambda}} \qquad (2.6)$$

Eq. 2.6 is the imbibition capillary pressure model proposed by Li and Horne (2001) empirically (for $D_f>2$).

In the case in which $b=0$, Eq. 2.1 can be reduced to: $P_c = p_{max}$. This equation may be considered a capillary pressure model for a single capillary tube.

One can see that Eq. 2.1, as a general capillary pressure model, could be applied in both complicated porous media and in a single capillary tube as well as in both drainage and imbibition cases.

## 2.4 EXPERIMENTAL MEASUREMENTS

The six core samples used in this study were the same as those used by Li and Horne (2003). The six core samples were from different wells at The Geysers geothermal field. The samples were irregular and too small to drill a plug for permeability measurements. The measured porosity of the core samples ranged from 0.1 to 4.0%. Capillary pressure curves of the six samples from The Geysers geothermal field were measured using the mercury-injection technique.

The surface tension of air/mercury is 480 mN/m and the contact angle through the mercury phase is $140^o$ (Purcell, 1949).

## 2.5 RESULTS

The experimental data from the six Geysers samples were used to verify the universal capillary pressure model (Eq. 2.3). The results are presented and discussed in this section.

Figure 2.1 shows a comparison between the experimental data and the universal capillary pressure model for the core sample SB15D_1. The points represent the experimental data and the solid line represents the results matched using the universal capillary pressure model (Eq. 2.3). Firstly, one can see that the capillary pressure curve is not a straight line on a log-log plot, which implies that the frequently-used Brooks-Corey capillary pressure model can not be applied to this geothermal rock. Secondly, the results show that the universal capillary pressure model (Eq. 2.3) can match the experimental data of satisfactorily.

Comparisons between the experimental data and the universal capillary pressure model for the other core samples are shown in Figs. 2.2-6. One can see that the universal capillary pressure model can match the experimental data well for all six of the Geysers core samples studied.
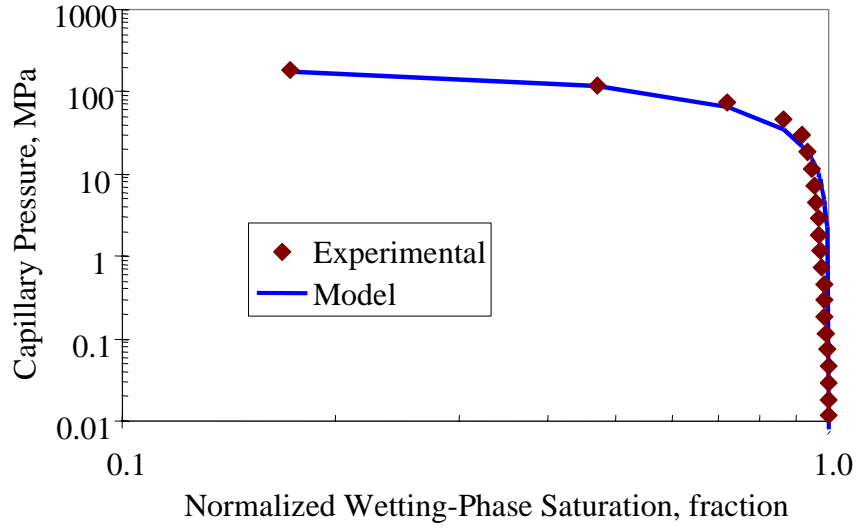
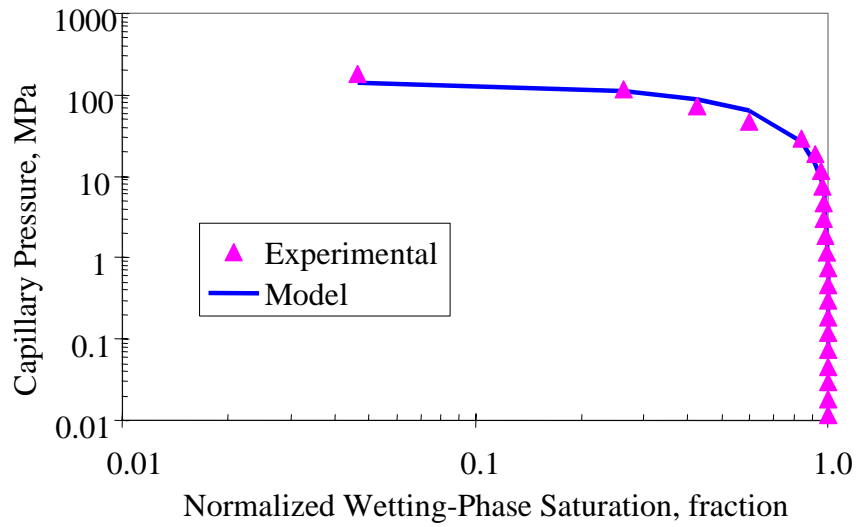*Figure 2.1:    Model fit to the experimental capillary pressure curve of The Geysers rock (No. SB15D_1).*



*Figure 2.2:    Model fit to the experimental capillary pressure curve of The Geysers rock (No. MLM_3).*
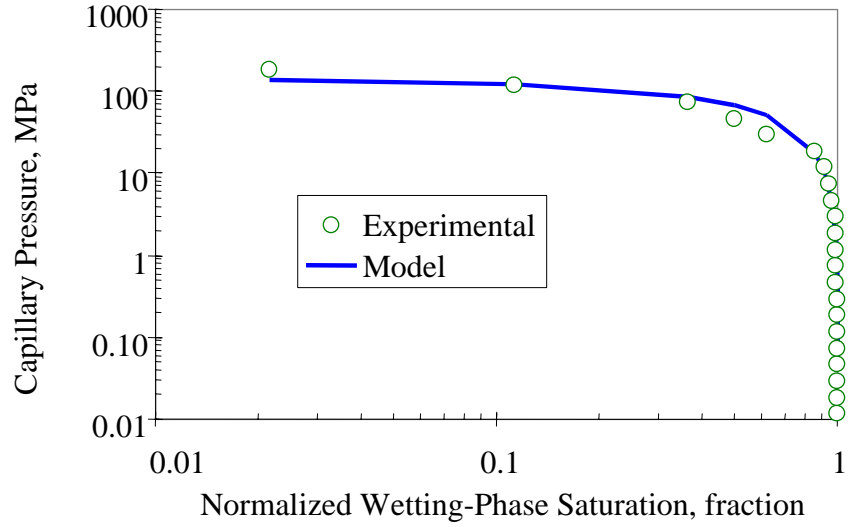
*Figure 2.3:    Model fit to the experimental capillary pressure curve of The Geysers rock (No. Pc_92).*
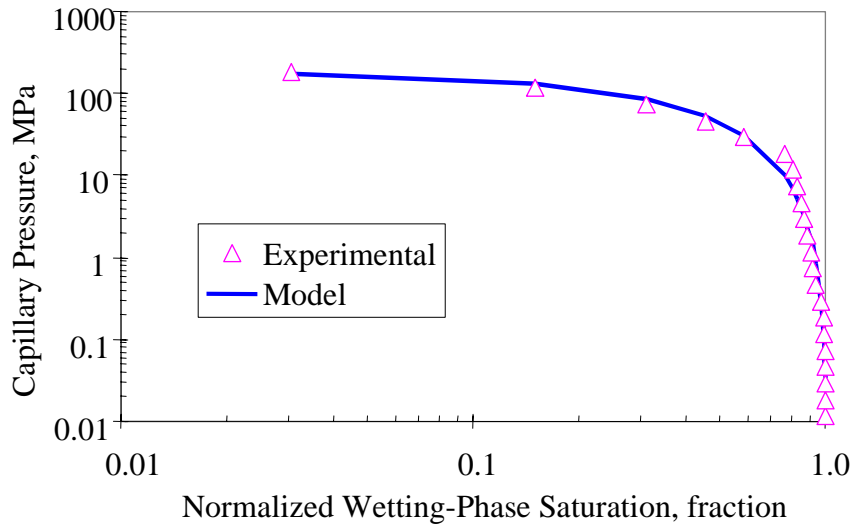


*Figure 2.4:    Model fit to the experimental capillary pressure curve of The Geysers rock (No. SB15D_2).*
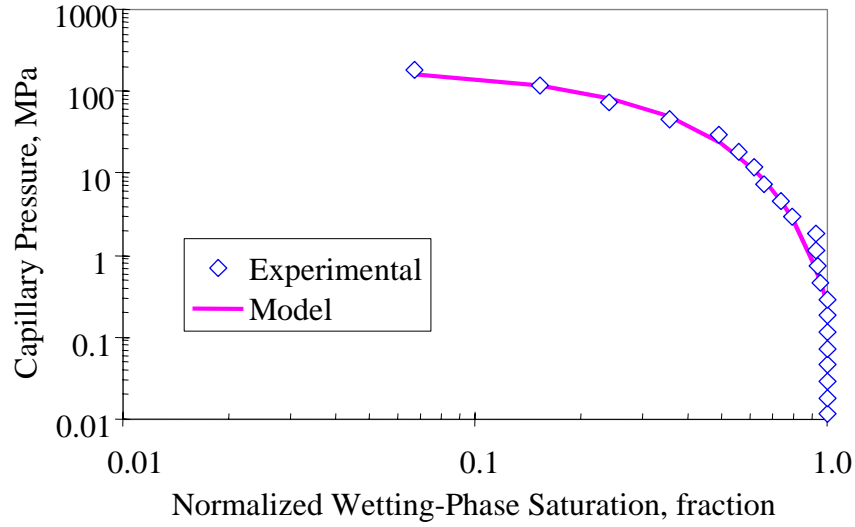
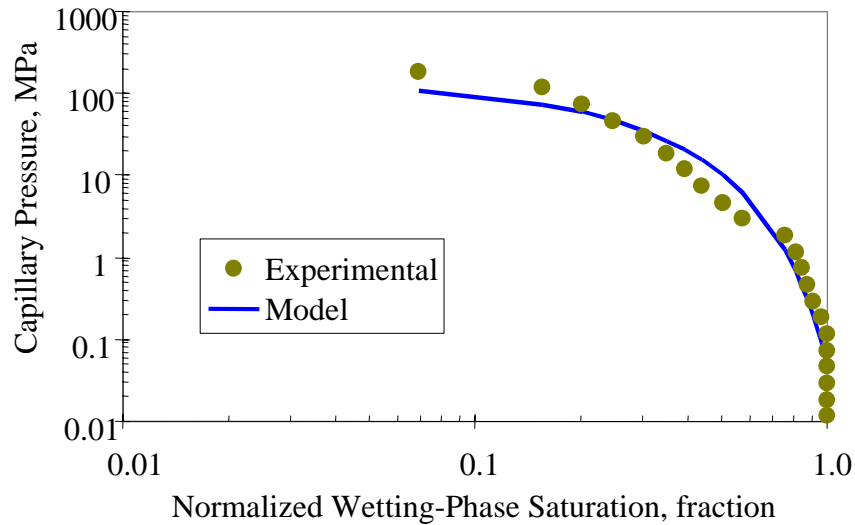Figure 2.5:   Model fit to the experimental capillary pressure curve of The Geysers rock (No. PRATI_5).



Figure 2.6:   Model fit to the experimental capillary pressure curve of The Geysers rock (No. CA1862_4).

The values of the three parameters, $p_e$, $p_{max}$, and $D_f$, were also inferred from the model match for all of the core samples and the results are listed in Table 2.1. Note that the values of the entry capillary pressure ($p_e$) are small. This may be because of the effect of the fractures in the rock.

The values of fractal dimension listed in Table 2.1 are different from those calculated earlier using another model (Li and Horne, 2003) for some of the core samples. However

the results are consistent with the visual observation of the heterogeneity shown in Figure 2.7. The greater the fractal dimension, the greater the heterogeneity. The values of fractal dimension shown in Table 2.1 demonstrate that the heterogeneity of the core samples decreases from left to right. This phenomenon can also be observed visually in Figure 2.7 based on the curvatures of capillary pressure curves.

*Table 2.1: Parameters inferred from model match.*

| Sample | SB15D_1 | MLM_3 | Pc_92 | SB15D_2 | PRATI_5 | CA1862_4 |
|---|---|---|---|---|---|---|
| $\phi$ (%) | 4.0 | 2.5 | 0.4 | 0.1 | 1.1 | 0.8 |
| $p_e$ (MPa) | 0.007 | 0.06 | 0.046 | 0.034 | 0.244 | 0.046 |
| $p_{max}$ (MPa) | 208.2 | 148.6 | 139.4 | 183.7 | 209.9 | 147.1 |
| $D_f$ | 3.120 | 3.069 | 2.957 | 2.483 | 2.224 | 2.188 |

One can see from Table 2.1 that there is no clear relationship between fractal dimension and porosity, or with the other parameters.
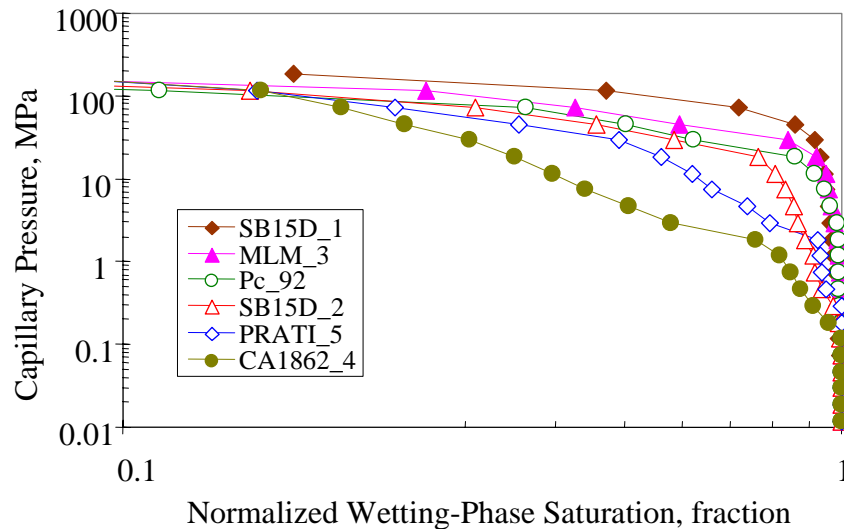


*Figure 2.7:    Capillary pressure curves of The Geysers rock samples.*

## 2.6 CONCLUSIONS

Based on the present work, the following conclusions may be drawn:
1. The universal capillary pressure model developed from fractal modeling of a porous medium can be reduced to the frequently-used Brooks-Corey model and the Li-Horne model in specific cases.
2. The universal capillary pressure model can match the experimental data from The Geysers satisfactorily in all the cases studied. However the Brooks-Corey model cannot match the experimental data in any of the core samples from The Geysers.

3. Fractal dimension, entry capillary pressure, and maximum capillary pressure can be evaluated from the match of the universal capillary pressure model to experimental data.

4. The inferred values of fractal dimension can be used to represent the heterogeneity of different rock samples quantitatively.

# 3. FRACTURED ROCK RELATIVE PERMEABILITY

This project is being conducted by Research Assistant Anson L. Villaluz, Senior Research Engineer Kewen Li and Prof. Roland N. Horne. The objective is to obtain measurements of steam-water relative permeability in real fractured rocks from geothermal reservoirs. This work is an extension of our earlier steam-water relative permeability studies, which have mostly considered artificially uniform and high permeability rocks. Now that the relative permeability mechanisms have been understood, we are ready to embark on the more difficult measurements using heterogeneous, low permeability rocks from geothermal reservoirs.

## 3.1 BACKGROUND

Steam-water relative permeability and capillary pressure are important data for geothermal reservoir engineering. The Stanford Geothermal Program (SGP) has succeeded in making fundamental measurements of steam-water flow in porous media and made significant progress in understanding this important process, which is central to the geothermal industry. One of the important problems left to undertake is the measurement of steam-water relative permeability and capillary pressure in geothermal rock (most of the previous study was conducted in high permeability sandstone as a well-controlled test material.).

Using our existing steady-state CT method, we have measured steam-water relative permeability and capillary pressure in rock with permeability above 100 md ($10^{-11}$ cm$^2$). We can obtain the in-situ fluid saturation simultaneously. For the geothermal rock with permeability smaller than 1 md ($10^{-13}$ cm$^2$), the steady-state CT method would work but it would take an extremely long time to conduct the experiments (weeks or even months). Hence the CT method is not practical to measure steam-water relative permeability in geothermal rocks.

To overcome this difficulty, we have embarked on a different approach, by measuring the relative permeability curves in separate sections. We have concluded from our experimental data (Satik, 1998; Horne *et al*., 2000; Mahiya, 1999; O'Connor, 2001; Li and Horne, 2000a) that steam-water relative permeability follows the Corey model and steam-water capillary pressure follows the fractal model (see Section 2). We can measure the end-point steam-water relative permeability and saturation in the geothermal rock with permeability smaller than 1 md using our existing steady-state CT method or the direct weighing method developed by Li *et al*. (2001). Then the whole curve of steam-water relative permeability can be obtained using the Corey model and the capillary pressure curve can be obtained using the fractal model. We plan to confirm the applicability of this approach first with nitrogen-water experiments, which are very much easier to conduct than the steam-water flows. This work was begun by Habana (2002), but ran into experimental difficulties.

The experimental study performed by Habana (2002) on a real fractured geothermal core showed results with pressure spikes occurring periodically during single-phase water injection. Erratic pressure spikes were observed during nitrogen-water relative permeability experiment in the same study. Some of the results are presented in Figures

3.1 and 3.2. The appearance of these transient effects indicated a difficulty with the experimental configuration, and prevented the measurement of relative permeability. In the continuation of this study, the apparatus has been redesigned and is being reconstructed to overcome these problems.
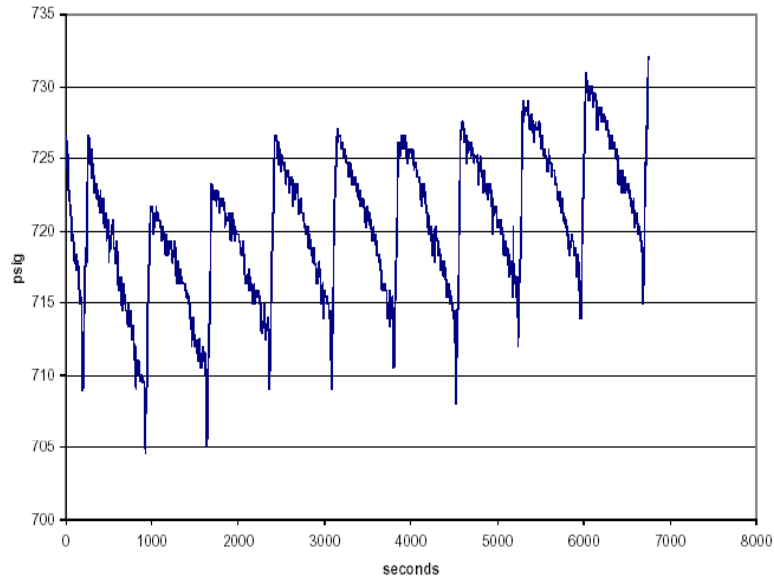


*Figure 3.1: Pressure at inlet during water injection. Constant water flow rate at 14 ml/min (Habana, 2002).*
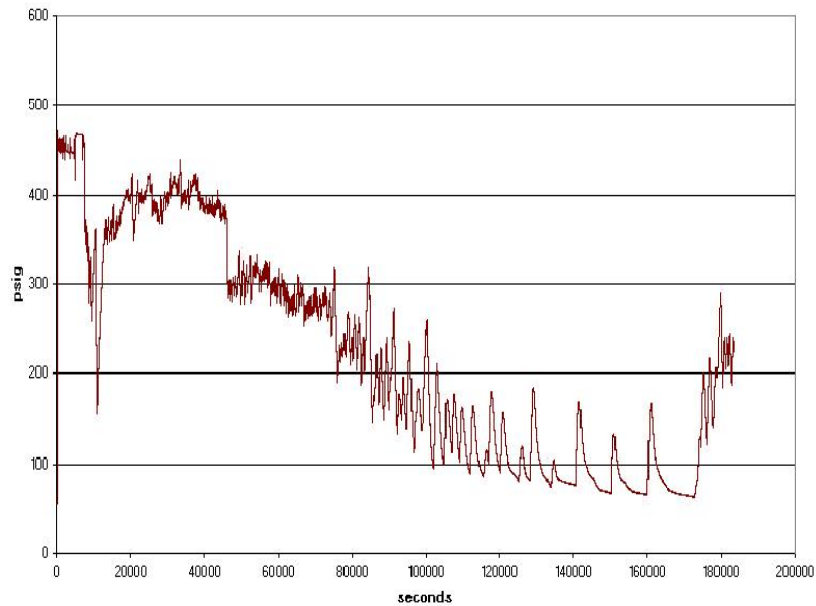


*Figure 3.2: Pressure at inlet for constant flow rate nitrogen-water experiment (Habana, 2002).*

36

## 3.2 EXPERIMENTAL METHODOLOGY

The rock permeability will be measured using nitrogen gas at room temperature. Gas permeability is a function of pressure. Therefore, the flow measurements will be conducted at a series of different mean pressures and taking into account Klinkenberg slip effect.

A new core sample has been obtained from a depth of 2440.5m at The Geysers geothermal field. The core is 8.9 cm in length and 4 inches in diameter.

Nitrogen will be flowed into the core at different confining pressures. Confining pressure from 500 to 850 psig can be reached by injecting nitrogen around the heat shrink tubing inside the core holder. To apply higher confining pressure water can be used in place of nitrogen.

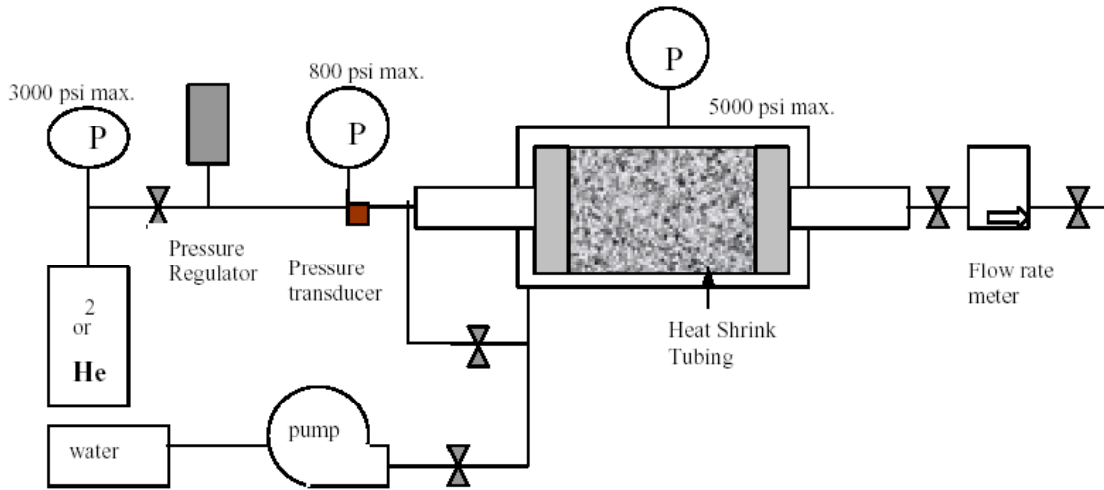A schematic illustration of the experiment is shown in Figure 3.3.



*Figure 3.3: Schematic representation of apparatus.*

## 3.3 THEORETICAL BACKGROUND FOR ELECTRICAL RESISTIVITY

Since X-ray CT measurement of saturation is likely to be difficult with such low permeability rocks, we are looking at the use of resistivity measurements to estimate saturation. In preliminary studies, electrical resistivity measurements were obtained to validate the relationship between resistivity and saturation via the Archie Equation.

This relationship can be represented by Equation 3.1:

$$I = bS_w^{-n} \tag{3.1}$$

where $I = R_t/R_o$ known as the resistivity index, $R_t$ is the resistivity at a certain saturation, $R_o$ is the resistivity at 100% water saturation, $b$ is some function of tortuosity, and $n$ is the saturation exponent. Empirically, $n = 2$ for Berea sandstone from previous studies.

## 3.4 NITROGEN-WATER RELATIVE PERMEABILITY EXPERIMENTAL METHOD

As a preparation to making relative permeability measurements of the geothermal core, and to have a deeper understanding of the relative permeability experimentation process, an apparatus was set up that is able to measure the data necessary to calculate relative permeability, and tested using Berea sandstone.

The steady state method for obtaining relative permeability data was employed. 1% NaCl solution and nitrogen gas were used as the two phases flowing in the core. A schematic diagram for the apparatus is presented in Figure 3.4. Electrical resistivity measurements were done simultaneously using an ordinary multimeter.
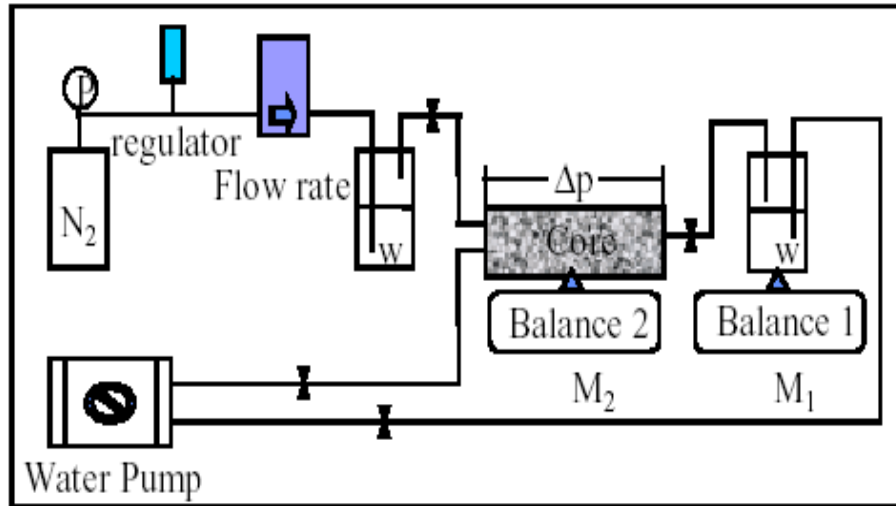


*Figure 3.4: Schematic diagram of steady state N₂-H₂O relative permeability test*

The core was put inside a rubber sleeve and two layers of heat-shrink tubing were further placed atop to prevent leaks. Saturation data were verified by weighing the core.

## 3.5 NITROGEN-WATER RELATIVE PERMEABILITY RESULTS IN BEREA SANDSTONE

Using Darcy's Law and assuming that the ideal gas equation applies, effective permeability data were calculated at different saturation points.

As in a usual steady-state relative permeability measurement, saturation was altered by adjusting relative injectivity, which is basically the ratio between the flow rates of brine and nitrogen entering the core.

The results of the relative permeability experiment are presented in Figure 3.5.
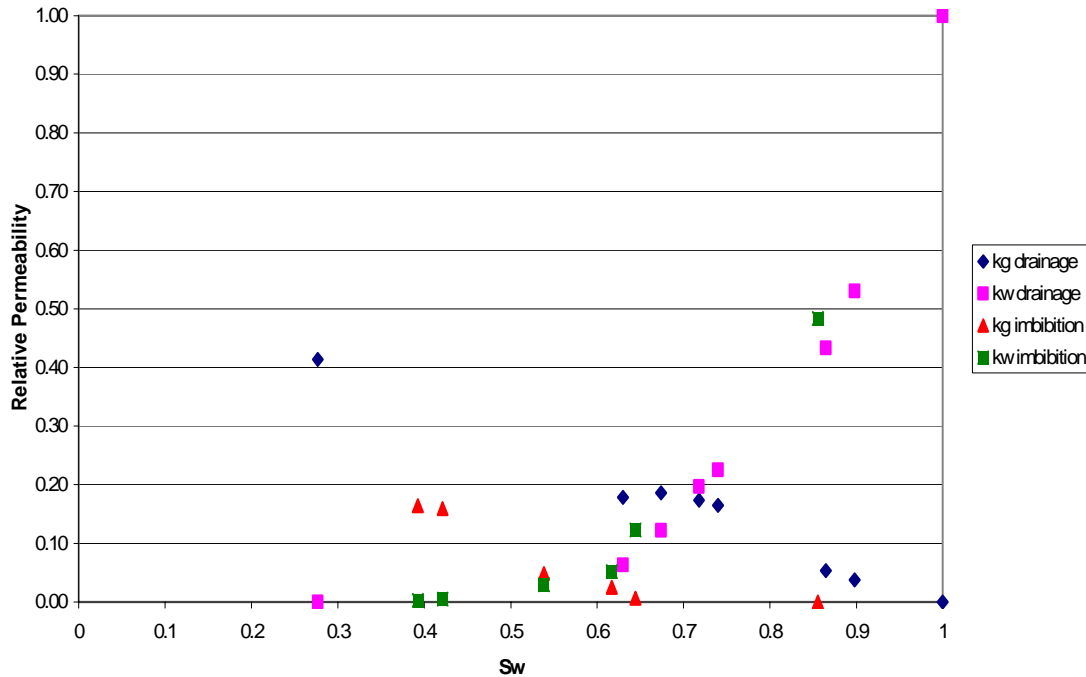


*Figure 3.5. Nitrogen-water relative permeability in Berea sandstone.*

The general trend of the results as seen in Figure 3.5 is acceptable. Relative permeability of each phase increases as the saturation of that particular phase increases. The results can be observed to follow the Brooks-Corey series model rather than the X-curve type model.

However, these observations must be verified by comparing the results with theoretical models.

Likewise, it can be seen from the same figure that relative permeability of the nonwetting phase during imbibition is considerably less than during the drainage process, probably due to trapping. On the other hand, the effect of saturation history to the wetting phase was not observed to be considerable, as expected.

## 3.6 RESULTS OF ELECTRICAL RESISTIVITY MEASUREMENTS WHILE PERFORMING RELATIVE PERMEABILITY EXPERIMENT

The result of using Archie's equation to correlate electrical resistivity with saturation while doing nitrogen-water relative permeability experiment is presented in Figure 3.6.

The results are found to be unconvincing and discrepancies can most probably be attributed to the use of a DC multimeter instead of an industrial AC resistance meter.
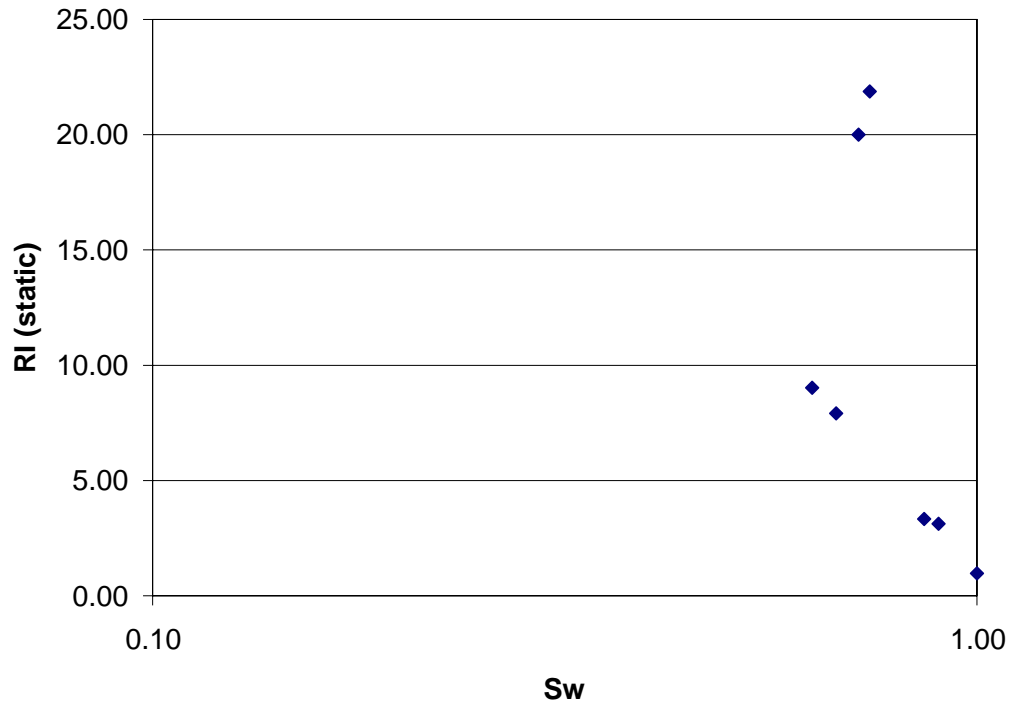


*Figure3.6. Archie's correlation.*

## 3.7 CONTINUING AND FUTURE WORK

An improved experimental apparatus for measuring nitrogen-water relative permeability in Berea sandstone was constructed. The core was put inside a customized stainless steel core holder to avoid leaks that were encountered earlier using just the rubber sleeve and heat-shrink tubing.

A resistance-measuring device employing AC voltage has been connected to the apparatus in place of the DC device used up until now. Nitrogen-water relative permeability measurements will be performed as resistivity data are measured simultaneously using the AC impedance meter. The steady-state method will still be applied to obtain these measurements.

After this preliminary experiment, the next challenge will be to measure relative permeability in fractured rocks. The experimental apparatus will be improved and nitrogen-water as well as steam-water relative permeability will be measured.

Lastly, pore network modeling will be applied with the aim of deriving relative permeability curves of fractured rocks, to verify results from fractured rock experiment.

# 4. REFERENCES

Arihara, N.: *A Study of Non-Isothermal Single and Two-Phase Flow Through Consolidated Sandstones*, Ph.D. dissertation, Stanford University, Stanford, California (1976).

Arihara, N., Ramey, J. and Brigham, W.E.: "Non-Isothermal Single and Two-Phase Flow Through Consolidated Sandstones," *SPEJ* (June 1976) 137-146.

Brooks, R.H. and Corey, A.T.: "Hydraulic Properties of Porous Media," Colorado State University, Hydro paper No.5 (1964).

Brooks, R.H. and Corey, A.T.: "Properties of Porous Media Affecting Fluid Flow," *J. Irrig. And Drain. Div.*, Proc. ASCE, IR2 (1966), Vol. **92**, p. 61-88.

Chen, C.-Y., Horne, R.N., and Fourar, M.: "Experimental Study of Liquid-Gas Flow Structure Effects on Relative Permeabilities in a Fracture," *Water Resources Research* (in press, 2004).

Chen, H.K.: *Measurement of Water Content in Porous Media Under Geothermal Fluid Flow Conditions*, Ph.D. dissertation, Stanford University, Stanford, California (1976).

Corey, A.T.: *Mechanics of Immiscible Fluids in Porous Media*, Water Resources Publications, Littleton, Colorado (1986).

Counsil, J.R.: *Steam-Water Relative Permeability*, Ph.D. dissertation, Stanford University, Stanford, California. (1979).

Diomampo, G.P.: *Relative Permeability through Fractures*, MS thesis, Stanford University, Stanford, California (2001).

Fourar, M., and Lenormand, R.: "A Viscous Coupling Model for Relative Permeabilities in Fractures," SPE 49006, paper presented at the 1998 SPE Annual Technical Conference and Exhibition, New Orleans, Louisiana, USA, September 27-30.

Fourar, M., Bories, S., Lenormand, R., and Persoff, P.: "Two-Phase Flow in Smooth and Rough Fractures: Measurement and Correlation by Porous-Medium and Pipe Flow Models," *Water Resources Research* (November 1993) Vol. **29** No. 11, p. 3699-3708.

Habana, M.D.: "Relative Permeability of Fractured Rock", MS report, Stanford University, Stanford, California, (2002).

Horne, R.H., Satik, C., Mahiya, G., Li, K., Ambusso, W., Tovar, R., Wang, C., and Nassori, H.: "Steam-Water Relative Permeability," Proc. of the World Geothermal Congress 2000, Kyushu-Tohoku, Japan, May 28-June 10, 2000.

Li, K.: "Universal Capillary Pressure and Relative Permeability Model Inferred from Fractal Characterization of Porous Media," SPE 89874, Proceedings of SPE Annual Technical Conference and Exhibition held in Houston, Texas, U.S.A., 26–29 September 2004.

Li, K. and Horne, R.N.: "An Experimental and Theoretical Study of Steam-Water Capillary Pressure," *SPEREE* (December 2001), p.477-482.

Li, K. and Horne, R.N.: "Experimental Verification of Methods to Calculate Relative Permeability Using Capillary Pressure Data," paper SPE76757 presented at the 2002 SPE Western Regional Meeting, Anchorage, Alaska, May 20-22.

Li, K. and Horne, R.N.: "Fractal Characterization of The Geysers Rock," Proceedings of the GRC 2003 annual meeting, October 12-15, 2003, Morelia, Mexico; GRC Trans. V. 27 (2003).

Li, K. and Horne, R.N. (2000a): "Steam-Water Capillary Pressure," SPE 63224, presented at the 2000 SPE Annual Technical Conference and Exhibition, Dallas, TX, USA, October 1-4, 2000.

Li, K., Nassori, H., and Horne, R.N. (2001): "Experimental Study of Water Injection into Geothermal Reservoirs," to be presented at the GRC 2001 annual meeting, August 26-29, 2001, San Diego, USA; *GRC* Trans. V. **25**.

Mahiya, G.: "Experimental Measurement of Steam-Water Relative Permeability," MS report, Stanford University, Stanford, California (1999).

Miller, F.G.: "Steady Flow of Two-Phase Single-Component Fluids Through Porous Media," *Trans. AIME* (1951) **192**, 205.

O'Connor, P.A.: "Constant-Pressure Measurement of Steam-Water Relative Permeability," MS report, Stanford University, Stanford, California (2001).

Pan, X., Wong, R.C., and Maini, B.B.: "Steady State Two-Phase Flow in a Smooth Parallel Fracture," presented at the 47th Annual Technical Meeting of the Petroleum Society in Calgary, Alberta, Canada, June 10-12, 1996.

Persoff, P., and Pruess, K.: "Two-Phase Flow Visualization and Relative Permeability Measurement in Natural Rough-Walled Rock Fractures," *Water Resources Research* (May 1995) Vol. **31**, No. 5, p. 1175-1186.

Piquemal, J.: "Saturated Steam Relative Permeabilities of Unconsolidated Porous Media," *Transport in Porous Media* (1994) **17**, p. 105-120.

Pruess, K., and Tsang, Y. W.: "On Two-Phase Relative Permeability and Capillary Pressure of Rough-Walled Rock Fractures," *Water Resources Research* (Sept. 1990) Vol. **26** No. 9, p. 1915-1926.

Purcell, W.R.: "Capillary Pressures-Their Measurement Using Mercury and the Calculation of Permeability", *Trans. AIME*, (1949), **186**, 39.

Romm, E.S.: *Fluid Flow in Fractured Rocks*, "Nedra" Publishing House, Moscow (Translated from the Russian) (1966).

Saidi, A. M.: "Simulation of Naturally Fractured Reservoirs," paper SPE 12270 in proceedings of the 1983 Symposium on Reservoir Simulation, San Francisco, CA, November.

Sanchez, J.M and Schechter, R.S.: "A Comparison of the Two-Phase Flow of Steam/Water and Nitrogen/Water Through an Unconsolidated Permeable Medium," SPE 16967, paper presented at the 62nd SPE Annual Technical Conference and Exhibition, Dallas, Texas, USA, September 27-30, 1987.

Satik, C.: "A Study of Steam-Water Relative Permeability," paper SPE 46209 presented at the 1998 SPE Western Regional Meeting, Bakersfield, California, May. 10-13.

Satik, C.: "A Measurement of Steam-Water Relative Permeability," Proceedings of 23rd Workshop on Geothermal Reservoir Engineering, Stanford University, Stanford, California (1998).

Scheidegger, A.E.: *The Physics of Flow Through Porous Media*, 3rd ed., University of Toronto, Toronto (1974).

Tsypkin, G.G. and Calore, C.: "Capillary Pressure Influence on Water Vaporization in Geothermal Reservoirs," Proceedings of 24th Workshop on Geothermal Reservoir Engineering, Stanford, Calif., 1996.

Urmeneta, N.A., Fitzgerald, S., and Horne, R.N.: "The Role of Capillary Forces in the Natural State of Fractured Geothermal Reservoirs," Proceedings of 23rd Workshop on Geothermal Reservoir Engineering, Stanford, Calif., 1998.

Verma, A.K.: *Effects of Phase Transformation of Steam-Water Two-Phase Relative-Permeability*, Ph.D. dissertation, University of California, Berkeley (1986).

Walker, W.R., Sabey, J.D. and Hampton, D.R.: "Studies of Heat Transfer and Water Migration in Soils," U.S. DOE Report, Colorado State University, Fort Callins, Colorado, April 1981.